AEROTHON 2024 – UNCREWED AIRCRAFT SYSTEM (UAS) DESIGN, BUILD AND FLY CONTEST

TEAM ARROW: AT2024-049

DESIGN REPORT FOR AEROTHON 2024

SCHOOL OF ENGINEERING, NIRMA UNIVERSITY

Team Members

Sr. No.	Name	Department	Role
1.	Neel Chhatrala	Electronics and Communication	Captain
2.	Jugal Gandhi	Electronics and Communication	Vice-Captain
3.	Mantra Patel	Mechanical	Mechanical Engineer
4.	Rutva Sheth	Mechanical	Design Engineer
5.	Shiv Vanara	Mechanical	Manufacturing Engineer
6.	Aayush Desai	Electronics and Communication	GCS operator
7.	Bhavya Goradia	Electronics and Communication	Software Engineer
8.	Het Patel	Electronics and Communication	Electronics Engineer
9.	Vishesh Brahmbhatt	Electronics and Instrumentation	Software Engineer
10.	Lakshya Rastogi	Electrical	Electrical Engineer

APPENDIX A
STATEMENT OF COMPLIANCE

Certification of Qualification
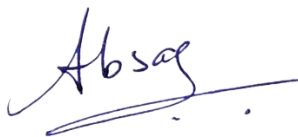
Team Name: Team Arrow

University/Institute: Institute of Technology, Nirma University.

Faculty Advisor: Dr. Absar M. Lakdawala

Faculty Advisor's Email: absar.lakdawala@nirmauni.ac.in

Statement of Compliance:

As Faculty Advisor, I certify that the registered team members are enrolled in collegiate courses. This team has designed the UAS for the SAE AEROTHON 2024 contest, without direct assistance from professional engineers, R/C model experts or pilots, or related professionals.

Signature of Faculty Advisor

Date 11-06-2024

Team Captain Information

Team Captain's Name: Neel Chhatrala

Team Captain's E-mail: 22bec017@nirmauni.ac.in

Team Captain's Phone: 9157544876

TABLE OF CONTENTS

ABBREVIATIONS

Short Form	Full Form
AOV	Angle of View
BEC	Battery Eliminator Circuit
BLDC	Brushless Direct Current
CAD	Computer Aided Design
CD	Coefficient of Drag
CG	Centre of Gravity
CL	Coefficient of Lift
CFD	Computational Fluid Dynamics
CFRP	Carbon Fiber Reinforced Plastic
CMOS	Complementary Metal-Oxide Semiconductor
CNN	Convolutional Neural Network
DHCP	Dynamic Host Configuration Protocol
EDA	Explicit Dynamic Analysis
EKF	Extended Kalman Filter
ESC	Electronic Speed Controller
FDM	Fused Deposition Modelling
FEA	Finite Elemental Analysis
FOS	Factor of Safety
FOV	Field of View
FPS	Frames per Second
FPV	First Person View
GCS	Ground Control Station
GNSS	Global Navigation Satellite System
GPS	Global Positioning System
GUI	Graphical User Interface
IP	Internet Protocol
MAVlink	Micro Air Vehicle Link
MDF	Medium Density Fiberboard
ODLC	Object Detection Localization & Classification
PDB	Power Distribution Board
PETG	Polyethylene Terephthalate Glycol
PID	Proportional Integral Derivative
PWM	Pulse Width Modulation
RPM	Rotations Per Minute
ROI	Region of Interest
RTL	Return To Launch
TLS	Transport Layer Security
UAS	Uncrewed Aerial System
UBEC	Universal Battery Eliminator Circuit
USB	Universal Serial Bus

ABSTRACT

This design report illustrates the innovative steps Team Arrow undertook in developing Uncrewed Aerial System (UAS) in preparation for the AEROTHON 2024 competition. The team applied generative design techniques to achieve structural excellence, various calculations were made to reduce weight without sacrificing functionality of UAS by integrating a mini carrier board and customized battery. Using advance image processing algorithm and single axis gimbal camera, UAS is capable of capturing wide field images and classification. By eliminating the requirement for an onboard computer, the team was able to streamline processes and increase computational efficiency by sending raw data to ground stations via Herelink. The optimization of the UAS's overall performance under strict weight limitations was given top priority during the development phase. Result of this dynamic factors makes UAS creative and prime among its category.

1. MISSION REQUIREMENT

MISSION 1
Objective: Survey a field, identify and classify objects based on shape, and count them using image processing and object detection algorithms.

MISSION 2
Objective: Autonomously survey a field, detect and count hotspots, identify, classify, and count objects based on shape using image processing and object detection algorithms.

MISSION 3
Objective: Navigate an obstacle course and deliver a payload to a target area manually.

MISSION 4
Objective: Autonomously survey a field, capture hotspots, identify a target, deliver a payload, and return to base without manual intervention.
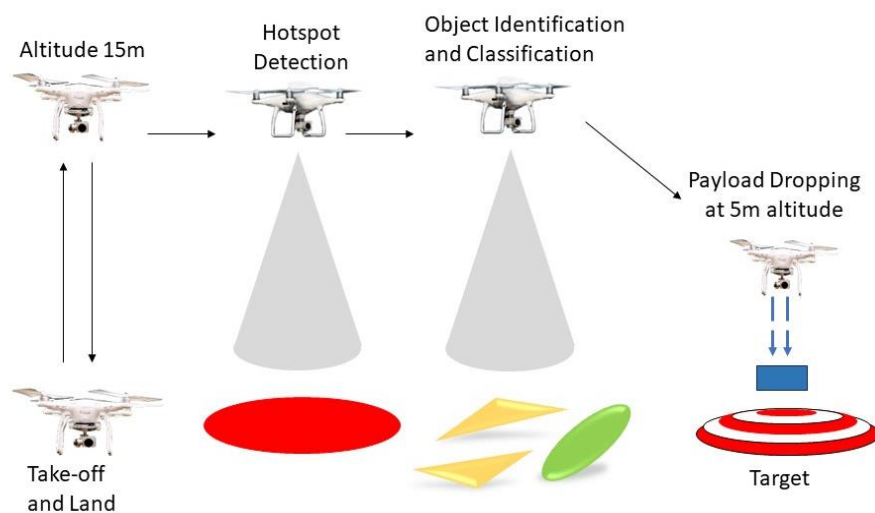
Figure 1: Flight Path for Aerothon 2024
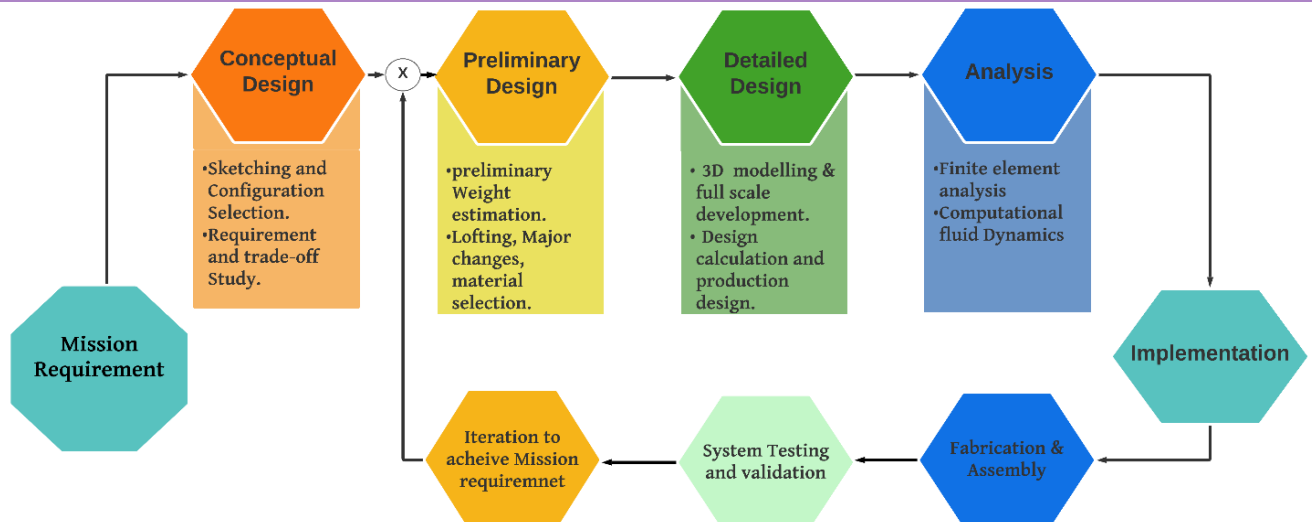
2. DESIGN PROCESS

Figure 2: Design Process

- Design process is an iterative process. Analysis of mission requirements results in development of fundamental ideas. Different configurations were explored through conceptual design, leading to the adoption of a well-balanced design that is in line with our requirements. As a part of detail design each component is carefully selected by rigorous testing and this iterative loop leads to optimization of UAS design.
- Previous endeavors had an impact in integration through fabrication, assembly, and thorough system-level testing. Subsystems were smoothly integrated, which allowed for incremental improvements with the goals of reaching the best possible weight, stability, and performance.

3. CONCEPTUAL DESIGN

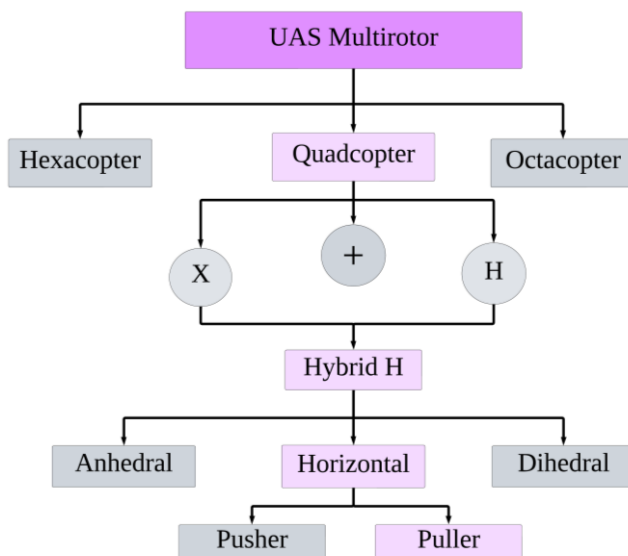The quadcopter configuration was selected for conceptual design

Figure 3: UAS Configuration Selection

Type
Quadcopter configuration was selected for balance between stability and maneuverability. As per the analysis of mission, quadcopter was the perfect configuration for given payload weight category.

Frame type
In quadcopter there are several frame types each with distinct purposes, as per the mission requirement H frame and X frame are optimal. X frame allows compactness in structural design which ultimately results in weight reduction and H frame has variable motor to motor distance along pitch and roll axis which gives desired stability and maneuverability.

Therefore, the most efficient configuration could be a hybrid of X and H frame (Figure 4).
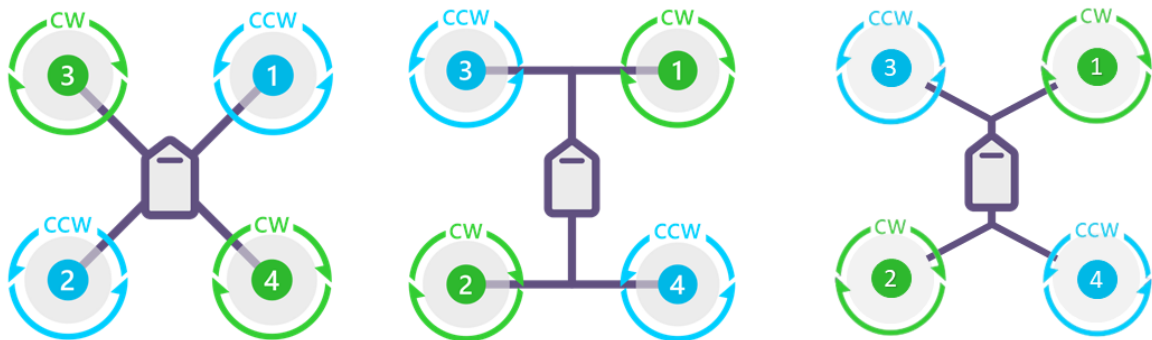
Figure 4: Configuration of Quadcopter i) X Frame ii) H Frame iii) Hybrid H Frame

Configuration
Pusher Configuration is more prone to heat generation due to which puller configuration is selected. Puller configuration draws air from above and propels it downwards. This meticulous design methodology was crafted to ensure the successful conception and construction of the UAS in alignment with mission requirements. Reference 1

3.1. PHYSICAL ARRANGEMENT OF ELEMENTS

The arrangement of the elements done in such way that center of gravity of Multirotor & Geometric center are concurrent which is shown is shown in Figure 5 & components are described in Table 1.

Figure 5: Exploded View of UAS

Table 1: Detailed description & purpose of the individual component used in UAS

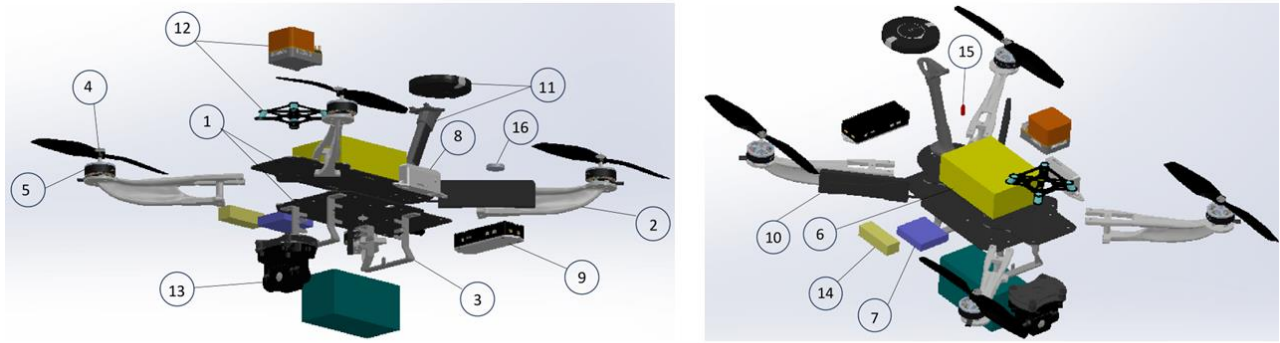| Sr. No.	Component	Description	Purpose
1.	Frame Hub	Consists of Top plate and Bottom plate made of Carbon Fiber reinforced Plastic.	a.) Top Plate: Provide housing for GPS, Battery, UBEC, Pixhawk, Camera & Herelink Antenna b.) Bottom plate: Provide housing for Herelink, Actuator, Payload & ESC.
2.	Rotor arm	Generative designed arm made by additive manufacturing method with PETG material	Arm creates linkage between housing plates & motor with adequate distance, providing the mounting for motor. Moreover, it supports the housing plates to be kept at required distance.
3.	Landing Gear	Aluminum Landing Gear	It provides clearance between ground and frame. Also provide surface for landing & take-off
4.	Propeller	8x4.5 inch	Propeller was used to generate lift by spinning & creating airflow
5.	Motor	iflight Xing X2806.5FPV	Provides thrust and rotates propeller
6.	Battery	Solid state Lithium-ion battery 6750 mAh	Power the electronic components on the UAS.
7.	ESC	4 in 1 ESC	Control motors speed
8.	Actuator	Linear Actuator	Payload dropping mechanism
9.	Herelink	-	Rc telemetry & Wi-Fi
10.	Herelink Antenna	-	Data Transmission
11.	GPS (with mount)	Here 3+	For navigation system
12.	Flight Controller	Pixhawk cube orange	Control system
13.	Camera	SIYI A2 Mini	Imaging system for FPV & object detection
14.	UBEC	Power brick mini	Powering auxiliary electronics
15.	Safety Switch	-	Prevent accidental arming
16.	Buzzer	-	Alarming system

4. DETAILED DESIGN

At detailed design stage, the design of real parts took initial projections into account, and every component underwent full-scale development. A "production design," consisting of designing, manufacturing, component performance, system testing, and finalising the weight and performance estimations, was completed.

4.1. PRELIMINARY WEIGHT ESTIMATION

The preliminary weight estimation was done before designing an UAS so as to get rough idea & to build a system within the weight constrain of 2 kg. The weight estimation is shown in Table 2

Table 2: Preliminary Quantity & weight estimation of the components to be used in UAS

Sr. No.	Component	Quantity	Weight (gm)
1.	Top Plate	1	50
2.	Bottom Plate	1	50
3.	Arms	4	160
4.	Bolts	45	95
5.	Stand-off	4	16
6.	GPS Stand	1	50
7.	Pixhawk Cube Orange	1	45
8.	Herelink	1	90
9.	Herelink Antenna	2	20
10.	Motors	4	213
11.	Propeller	4	28
12.	Camera	1	85
13.	GPS	1	50
14.	Buzzer & Safety Switch	1	18
15.	ESC	1	25
16.	Battery	1	500
17.	UBEC	2	30
18.	Wires	-	150
19.	Drop Mechanism	1	25
20.	Payload	1	200
Total			1900

4.2. THRUST REQUIRED

A minimum thrust-to-weight ratio is required for safe UAS operation, calculated based on weight estimation to ensure sufficient thrust to overcome weight and sustain flight. As the preliminary weight of the UAS is 1.9kg and assuming the thrust required to be of 6 kg for smooth accomplishment of the mission, minimum thrust of 1.5 kg is required in one motor. The thrust required for the UAS depends upon the motors current draw and banking angle while cruising on an axis, so considering higher thrust to weight will provide a smooth and easier control over the UAS in comparison with lower thrust to weight ratio. Ideal thrust to weight ratio of the UAS for our frame is

T/W	Task
>1	To hover the multirotor
>2	Ideal T/W ratio for Multirotor

$$\frac{Thrust}{weight} = \frac{6}{2} = 3:1$$

4.3. SELECTION OF PROPULSION SYSTEM

The propulsion system and its selections are crucial for optimal performance, making it indispensable in overall drone design. Detailed propulsion selection is as below

4.3.1. MOTOR SELECTION

After comparing Brushed DC & Brushless DC Motor as shown in Figure 6 the BLDC motor was chosen.
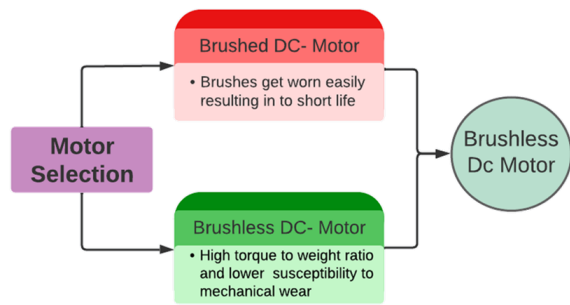

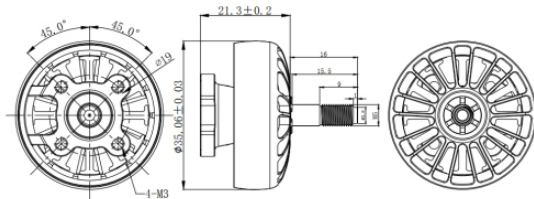**Figure 6: Comparison of Brushed DC & Brushless DC Motor**

After analyzing various BLDC motors and considering factors like KV rating, load current, maximum continuous current, maximum continuous power, motor weight, propeller size, thrust, and efficiency we concluded a list of motors & further compared them as shown in Table 3.

Table 3: Comparison of BLDC motors based on various parameters

Parameters	Sunny Sky X2212 V3	iFlight Xing X2806.5	Emax ECO II2807
Weight (gm)	57	**51.2**	60
Thrust(gm-f)	1650	**2426**	1891
Load Current (Amp)	29	**30.24**	46.2
Operating Voltage(V)	16.8	**16.8**	16.8
KV ratings (RPM/V)	980	**1300**	1700
Suggested propeller diameter (inch)	10	**8**	7

Figure 7: 2D Drawing of the iFlight Xing X2806.5 motor

Among above three motors listed EMAX Eco II 2807 was rejected due to its higher KV rating which increases the RPM per motor and reduced the efficiency of the motor while in case of Sunny Sky the lower thrust and higher weight doesn't meet the mission requirement. Thus, the Xing 2806.5 was selected as it gave higher thrust, lower weight and less current draw while cruising and banking which improves the efficiency of the UAS.

4.3.2. ELECTRONIC SPEED CONTROLLER (ESC)

An Electronics speed controller is a electrical circuit which regulates the speed of the electric motor. It consists of MOSFET as a primary component which is an electronic switch that turns ON/OFF upon getting a specific frequency signal provided by the flight controller. We chose t-motor f55A pro F3 4 in 1 ESC for our quad-copter considering the parameters of motor's max current draw, it's compactness in dimension its inbuilt BEC and a 20% of safety factor from maximum current of the motor. Furthermore, it also acts as a power distribution board (PDB). The above ESC has D-shot protocol which enables fast communication between the ESC and flight controller.

The specifications of the selected ESC are as shown in Table 4:

Table 4: Specification of four in one ESC selected for UAS

Model	Current	Peak Current	BEC	Battery	Weight	Size
F55A PRO II •F3 6S 4 in 1	4*55 Amp	4*75 Amp	10 V 2 Amp	3-6S	17.5 gm	45*41* 7.3mm

4.3.3. PROPELLER

Propeller converts rotary motion into linear thrust. Spinning the propellers creates an airflow pushing downwards which ultimately creates a pressure difference between the sides of the blade. Pressure varies with the speed of rotation which is controlled by ESC. Reference 2

For our specification we have used different propellers and the test results are as below.

Table 5: Comparison of propeller with 2 & 3 blade that were compatible with motor & has market availability

Prop (Inch)	Blade	Voltage(V)	Load Current (Amp)	Thrust (gm-f)	Power (Watt)	Efficiency
7x4	3	24	48.18	2586	1156.3	2.23
8x4.5	**2**	**16**	**48.59**	**2426**	**777.4**	**3.12**

As per initial calculation the Xing2806.5 motor was best fit for the UAS thus the team has to choose the propeller compatible with the motor. Thrust bench test was conducted for the two-blade and three-blade propellers, two-blade propeller was selected due to its higher efficiency, low power requirement & higher durability & lower weight.

4.4. UAS DESIGN & SIZING

4.4.1 FRAME HUB

Frame hub is the most crucial component of UAS due to all components were assembled on the frame therefore, it must be structurally sound, light weight and free from the vibration caused by the motor.
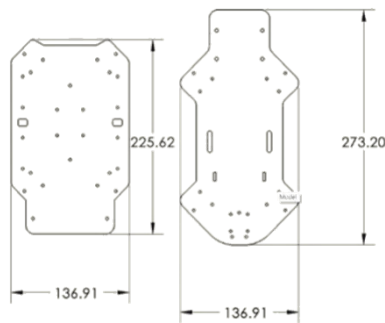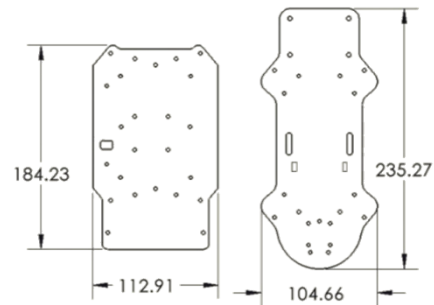

Figure 8: Initial frame hub design

Figure 9: Final frame hub design

Initially, the team came up with design based on the mission requirements, which is shown in Figure 8. The quadcopter plates were carefully designed to make it simple to accommodate all electronic parts. It consisted of two precisely chosen 1.5 mm thick plates an upper plate and a base plate made of carbon fiber sheets woven into a twill weave that were selected for their ideal strength-to-weight ratio and required stiffness. The base plate held the Herelink, Actuator, Payload, and ESC, while the top plate housed the GPS, Battery, UBEC, Pixhawk, Camera, and Herelink Antenna. The 30mm vertical distance between the two plates was established to accommodate electronics components, while lowering the base plate contributes to a lower center of gravity (C.G), thereby enhancing drone stability. Additionally, assembly of these plates was done by integrating rotor arm.

For optimal stability in a frame hub design, an aspect ratio greater than 1.5 is desirable, with a ratio of 2 or higher preferred for enhanced stability. Initially, our design achieved an aspect ratio of 2. However, by leveraging a battery type change, our team successfully optimized the frame hub, resulting in a revised design as shown in Figure 9 that not only reduced weight but also achieved a higher aspect ratio of approximately 2.2. This improvement significantly enhances the stability of the aircraft, making it particularly suiTable for surveillance applications where steady flight is crucial

4.4.2. PROPELLER CLEARANCE

The drone's size was initially used to determine the appropriate propeller size. The propeller diameter was chosen to maximize the frame's surface area while avoiding tandem aerodynamic interference, where the rotor vortices interact. To prevent propeller interference, the minimum distance between motor centers should exceed the propeller diameter. According to computational analysis, the distance between propellers was estimated to be at least 1.15 times the diameter (1.15D), currently distance between two motors.

Figure 10 are the pictorial representation for initial & Final Design. In preliminary design minimum distance between two motor is 292.88mm & for final design it is 280mm & the required distance is 233.68mm
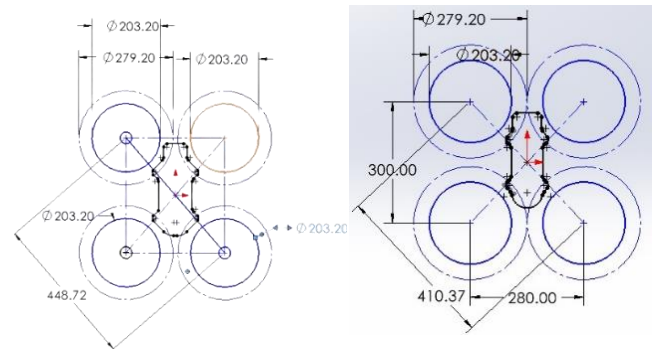

4.4.3. WHEELBASE

As illustrated in Figure 10, the wheelbase,

defined as the distance between the diagonally opposite motors, measures 448.72 mm. This dimension was carefully calculated to accommodate the closed hybrid H-frame design, with an angle of 50º between the arms in reference with roll axis. Additionally, the motor-to-motor distance was optimized to ensure unobstructed clearance for the front camera. By considering the frame size and wheelbase, we calculated the optimal rotor arm length to be 130 mm, striking a balance between stability, maneuverability, and camera visibility. Due to changes in frame hub eventually it leads to decrease in our wheel base.

4.4.4. ROTOR ARM DESIGN
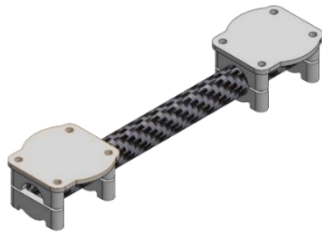
For the rotor arm design, the team initially utilized a circular carbon fiber rod. However, as the assembly process necessitated flat support for attaching motors and securing to the plates, a 3D printed arm clamp was incorporated as shown in Figure 11. This clamp featured a circular inner cross-section and a square outer cross-section to meet these requirements.

Figure 11: Rotor arm design with Circular CFRP rod incorporated with 3D printed Clamp.

During prototype testing, it became evident that orienting the 3D printed clamp were connected using fasteners that tends to loose with time & more components means higher DOF which means more vibrations, resulting in unwanted rotations. This prompted the exploration of a new design where the carbon fiber rod underwent morphing, featuring a circular cross-section in the middle and a square cross-section at the ends as shown in Figure 12. However, the high cost of manufacturing and the observation of excessive strength and weight in the rod led the team to seek alternatives.
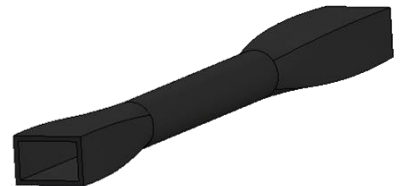
Figure 12: Morphed CFRP rotor arm

Subsequently, the team opted for a novel approach: utilizing generative design through Fusion 360 to craft the arm shown in Figure 13. This technique allowed for the removal of material in areas with lower stress, optimizing both strength and weight. Considering the complexities of the design, the team evaluated two manufacturing options: 3D printing and injection molding.

Table 6 shows the comparison of all the designs and manufacturing process.

Figure 13: Rotor arm designed by generative design using Fusion 360

Table 6: Comparison of various rotor arm design

Design	Carbon fiber Rod with motor mount clamp	Morphed Carbon Fiber rod	Injection Molding of Generative Design	3D Printing of Generative Design
F.O.S.	3.4	5.2	6	3.6
Cost	3000 INR	10,000 INR	15,000 INR	3000 INR

Team finalized 3D printing as Injection molding is very expensive for the prototyping. Injection Molding may be used for mass manufacturing. Reference 3

4.4.3 LANDING GEAR

The landing gear system was designed and optimized with consideration for the maximum payload capacity and structural integrity required to withstand ground impact. A horizontal base plate was integrated into the design to provide a sTable and level surface for touchdown, ensuring minimal shock transmission to the UAS. Initially, four stand-offs were incorporated into the design to securely fasten the payload to the base plate, serving as a critical component of the dropping mechanism. Base was increased to overcome topple effect & it also distributes load.
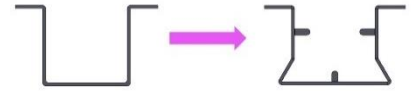
Figure 14: Change in Landing gear design

However, through a process of design optimization and structural analysis, the team identified an opportunity to consolidate functionality and reduce overall weight. By redesigning the landing gear (Figure 14) to inherently possess the structural robustness necessary to support the payload (Figure 15), the need for separate stand-offs was eliminated. This design refinement not only reduced the overall system mass but also enhanced the overall structural efficiency and reliability of the landing gear system.
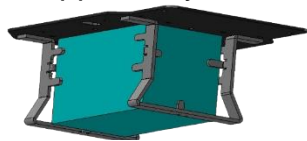
Figure 15: Final Landing gear design that could hold payload.

4.5 UAS PERFORMANCE

For obtaining desired endurance Power system selection is a crucial factor.

4.5.1 POWER REQUIRED ESTIMATION
Estimation of power required was done on the basis of power consumption of all the Components needed for the particular UAS as shown in Table 7.

Sr. No.	Component	Operating Voltage (Volt)	Operating Current (Amp)	Power Consumption (Watt)
1.	Flight Controller	5	2	10
2.	Motor + ESC	16	32.8	525.5
3.	Herelink	10	0.4	4
4.	Camera (SIYI A2 Mini)	12	0.16	2
5.	Servo Motor	5	0.6	3

Table 7: Estimation of power required based on electrical component

Total Power Consumption = 544.5 Watt

Power consumption (excluding motor) = 19 watt
- Main power consumption on drone will be of motor. Now, for different situations the current draw of motor will be different. Considering extreme cases, we have calculated total power consumption of UAS.
- For these calculations we have performed vector calculations in 3D dimension means required thrust of motor when UAS is having specific lean angle for hovering and cruising in all different situations. They are classified as below,

1. For hovering
- As per design of our UAS stability in roll axis is greater than stability in pitch axis so UAS will get leaner angle when windspeed is along the roll axis.
- Windspeed of 10 m/s is extreme condition for UAS as per our analysis. So, at 10m/s it will have maximum of 10 degree of lean angle so UAS requires 533 gm of thrust including buffer. At specified thrust current draw of each motor will be 7.5A.

2. For cruising
- Cruising against wind along pith axis: As per mission analysis cruising speed of our UAS will not be greater than 7 m/s and considering maximum windspeed of 10 m/s maximum lean angle of UAS will be 17 degrees at specified angle thrust required per motor will be 548 gm which draws 7.65A current.

- Cruising against wind along roll axis: This will be most extreme condition which UAS has to face during mission. Considering 10 m/s windspeed along roll axis means maximum angle of 10 degree in roll axis with 7 m/s speed of UAS along pitch axis so 7 maximum 7 degree of angle on pitch axis by calculating required thrust for this situation by 3D vector calculation will require 825 gm of thrust which draws 8.2A of current.

So, considering every extreme situation for cruising and hovering including buffer current draw of each motor will not exceed 8.2 A. Detailed calculations are mentioned in Reference 4

4.5.2 POWER SYSTEM (BATTERY) SELECTION

For optimum flight time there should be a balance between mAh, no. of cells, C rating, and weight of the battery.

For preliminary selection of the power system the team used Li-Po battery of 6200mAh 25C 4S considering parameters of configuration, maximum discharge, power required estimation while the above battery was selected as a preliminary battery for the UAS. Parallelly, the team was researching and designing a customized battery

Figure 16: Comparison of Various battery types

with a chemistry that gives benefits of both lithium ion and polymer battery i.e., solid state li-ion battery which gives sufficient weight reduction and enhanced endurance (Figure 16). As when the team successfully designed and finalizes the configuration, mAh, max discharge current, the team was also successfully able to manufacture this battery and test result show that the endurance was increased by 18% while the weight of the battery got reduced by 20% with increase in mAh of the preliminary one. Thus, the final battery configuration is 6750mAh 15C 4S with a weight of only 450 grams. Reference 5

Table 8: Battery configuration

	Preliminary	Final
Type	Li- Po	Solid state Li-ion
Configuration	4 Cell	4 Cell
Capacity (mAh)	6200	6750
C rating(C)	25	15
Max. Current Discharge (Amp)	155	101.25

4.5.3 ENDURANCE ESTIMATION

Given a maximum mission time constraint of 10 minutes, a minimum battery reserve of 20% is required to ensure mission completion without depletion. This necessitates an estimated endurance of 12 minutes, taking into account potential contingencies and ensuring a safe operating margin.

As per UAS configuration,

$$Endurance = \frac{Wh * 60}{Total\ Watt}$$

Watt-hour defines how much amount of power can a battery deliver over a certain period of time.

$$Watt\ hour\ rating = No.of\ cell * nominal\ volatge * battery\ capacity = 4 * 3.7 * 6.75 = 99.99\ Wh$$

The endurance does not depend only on power consumption by the motor and auxiliary electronics but it also depends upon at what throttle percentage what the thrust provided and current is drawn thus from above section at 40% the UAS has enough thrust to hover at a

required current of 5A per motor. While, at cruising according to thrust bench result and mechanics the required thrust per motor is 825 gm which draws maximum current of 8.2A per motor i.e. total of 32.8A by the UAS.

So, the estimated endurance of the UAS is

$$endurance = \frac{Wh*60}{total\ watt\ consumed} = \frac{99.99*60}{544.5} = 11\ minutes$$

All the calculation of propulsion & power system were verified using E-calc software. Reference 6

4.6. MATERIAL SLECTION, FABRICATION & ASSEMBLY

FRAME HUB

For the Quadcopter's frame, MDF and aero-ply were initially considered due to weight restrictions. However, their utilization was impractical due to environmental effects over time. Following that, composite materials came out as feasible substitutes, used for their high strength-to-weight ratio and lightweight design. Additionally, carbon fiber's natural resistance to heat has solidified its importance as a key material in aviation.

Table 9: Comparison of various material for frame hub based on Density, strength to weight ratio & cost

Properties	MDF	Aeroply	CFRP
Density	0.81 g/cc	0.61g/cc	1.55g/cc
Strength-to-weight ratio	Medium	Low	High
Cost	Low	Medium	High

For the fabrication of CFRP plate 1.5 mm thickness square plate was purchased & then it underwent CNC process for the required shape and to achieve precise cuts. Reference 7

ROTOR ARM

The rotor arms were designed for production through 3D printing (FDM). To determine the most suiTable material, a comparison was conducted across various parameters, outlined in Table 10

Table 10: Comparison of material for rotor arm based on strength to weight, printing difficulty, temperature resistance & cost

Properties	PLA	PET-G	ABS	PET-G + 15%C.F.
Strength-to-weight ratio	Low	Medium	High	High
Printing difficulty	Low	Low	High	Medium
Temperature resistance	Low	Medium	High	Medium
Cost	Low	Low	High	Medium

Based on the comparison carbon fiber infused PET-G was selected for fabricating rotor arm. Reference 7

LANDING GEAR

Landing Gear were designed so as to overcome impact load. The materials considered for landing gear are MDF, Aluminum & CFRP and Table 10 shows the comparison.

Table 11: Comparison of materials for landing gear based on Density, strength to weight ratio, cost & fabrication difficulty

Properties	MDF	Aluminum	CFRP
Density	0.81 g/cc	2.7 g/cc	1.55g/cc
Strength-to-weight ratio	Low	Medium	High
Cost	Medium	Medium	High
Fabrication difficulty	Easy	Easy	Difficult

For fabrication initially the horizontal plate was laser cut as per 2D drawing & further it was bent in U shape.

FABRICATION & ASSEMBLY

For the UAS, the fabrication process for the frame hub, rotor arm & landing gear was previously described. Other components were procured directly. Assembly involved mounting various electronic components onto both the base plate and upper plate as predetermined using fasteners and adhesives. The rotor arm served to connect both plates, with motors and propellers affixed to the opposite end. Stand-offs were then mounted beneath the base plate to support the payload, effectively serving as landing gear.

4.7 SUBSYSTEM SELECTION (COMMUNICATION SYSTEM, CONTROL & NAVIGATION SYSTEM & OTHER AVIONICS/ SENSORS)

The below given block diagram shows complete subsystem and its signal flow.
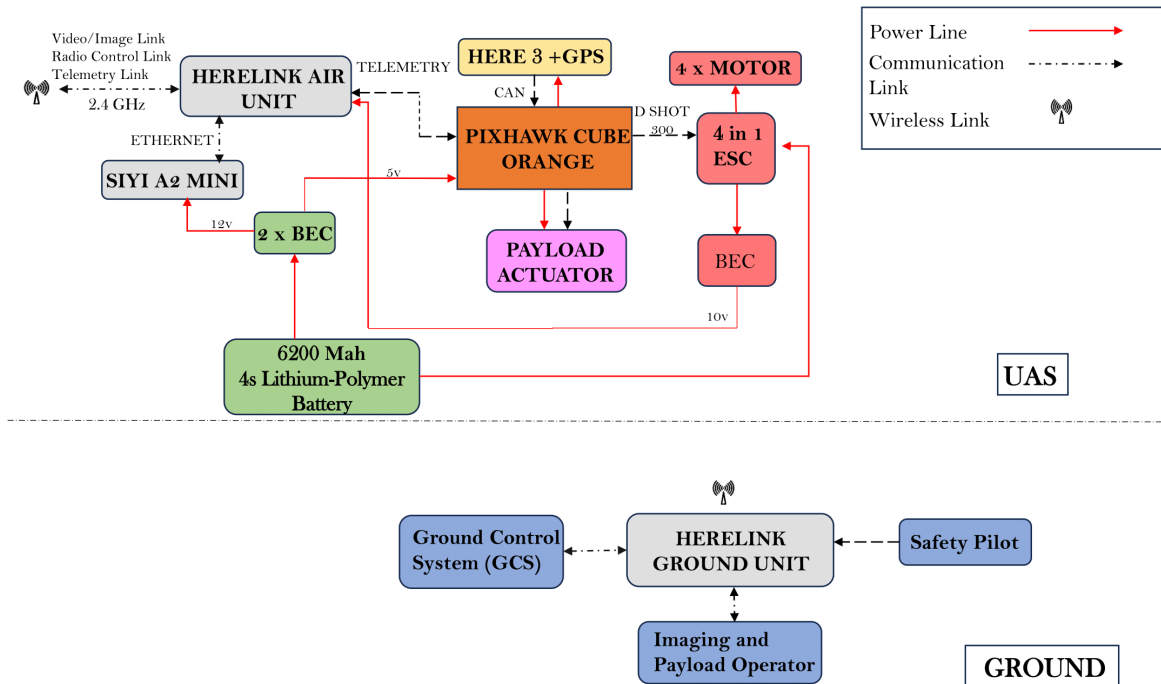
Figure 17: System Overview & block diagram for UAS

4.7.1 COMMUNICATION SYSTEM

As per the requirement of the mission robust communication is essential for performing the mission without any system failure. Three communication links on UAS are mandatory for it.

1) Telemetry link,

2) Radio Control link

3) Video-Image Transmission link
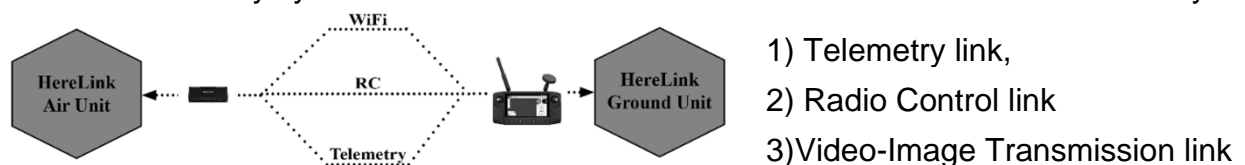
Figure 18: Communication system

Table 12: Advantages & Disadvantages of using herelink & separate module for each link

Herelink	Separate Module for Each Link
• Requires less space on frame hub for mounting • Less Power Consumption • Weight reduction • No signal interference due to single module	• Need more space on hub for mounting • More Power Consumption • Increase in weight • Signal interference arose due to separate component

So, by concluding from Table 12, using a single module is a better option. Therefore Herelink 1.1 is used as a Telemetry link, Radio Link and Video-Image transmission link. It consists of a Herelink-Air unit for UAS and Herelink-Ground Unit as a ground control station.

Herelink-Air Unit (Figure 19)
- Telemetry link protocol: UART
- Radio Link Protocol: Serial Bus (S.BUS)
- Video-Image Transmission Link Protocol: Ethernet (ETH)

Range of 16 Kms with low latency of telemetry data transmission with high efficiency of less than 1% data packet loss and allowing access of live stream with a low latency of 110 millisecond delay on Ground unit makes herelink a better option. Furthermore, the ground control unit of Herelink could function as a standard RC transmitter and support software such as Mission Planner and QGroundControl, acting as the main GCS. The ground unit could also create a hotspot, allowing other computers to connect to its network and share data from the UAS. The module's manufacturer claimed a range of 16 Kms, and the team successfully tested it for distances exceeding 2 kilometers using all three links simultaneously.
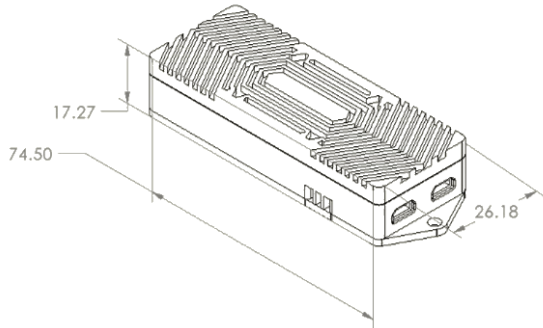

Figure 19: Herelink Module

CONTROL & NAVIGATION SYSTEM

CONTROL SYSTEM

Pixhawk Cube Orange (Figure 20) is a general-purpose flight controller which is fully customizable for any type of UAS Task and application. It can communicate with a Companion computer using a serial port inbuilt in it.

Table13 shows the technical specifications of Pixhawk cube orange
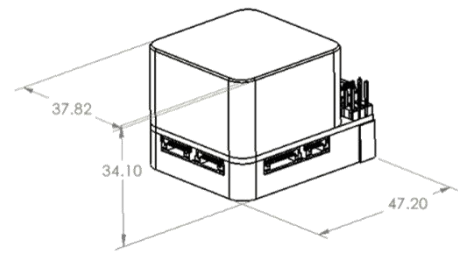
Figure 20: Pixhawk Cube Orange

Table 13: Specification of Pixhawk Cube Orange – flight controller

Processor	Main processor: 32-bit ARM® STM32H753 Cortex®-M7 Co-processor: STM32F103
Ram	400 MHz 1 MB RAM/2 MB Flash
Barometer	MS5611
Accelerometer/gyro	ICM42688 ICM20948
Magnetometer	AK099916
Interfaces	5x UART serial ports

We considered every possible environmental disruption when designing the control system for our UAS. By continuously modifying the motors' speeds, a PID (Proportional-Integral-Derivative) closed loop control system in Arducopter for a quadcopter guarantees steady and accurate flight which is as shown in Figure 21. The way this system works is it compares the orientation and location of the quadcopter to the desired state that is established by the pilot or by directions sent by itself. The three components of the PID controller are the derivative term, which predicts future errors based on the rate of change, the integral term, which accumulates past errors to correct systematic bias, and the proportional term, which responds to the current error. The PID controller calculates the error between these states. These three phrases work together to provide a corrective signal that the PID
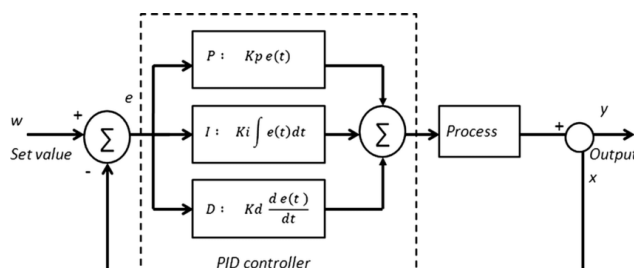
Figure 21: PID algorithm in flight controller.

controller uses to modify each motor's throttle and stabilize the quadcopter. The quadcopter may be adjusted in real-time to ensure that it reacts quickly to environmental disturbances and maintains a smooth and controlled flying thanks to this continuous feedback loop. Reference 8

To fly well, with tight navigation and reliable performance in the wind, tight tuning of autopilot parameters is mandatory. From freedom of axis of drone tuning of Pitch axis, roll axis and Yaw axis will provide indispensable control over drone. Each axis has their Proportional, Integral and Derivative Gain tuning Sequence of these parameters are as follows

Post-Test Flight Tuning and Optimization Report

1. Manual Tuning: Manual tuning was performed to establish a sTable baseline PID for autotuning, ensuring a robust foundation for automatic tuning.

2. Autotuning Sequence: The autotuning process was executed in the following sequence:

- Roll axis
- Pitch axis
- Yaw axis

This sequence ensured optimal tuning for each axis.

Refined Autotuning: The roll and pitch axes were autotuned again to further refine the PID gain, resulting in optimal performance and precision. We can observe sTable PID by analyzing step response shown in Figure 22.
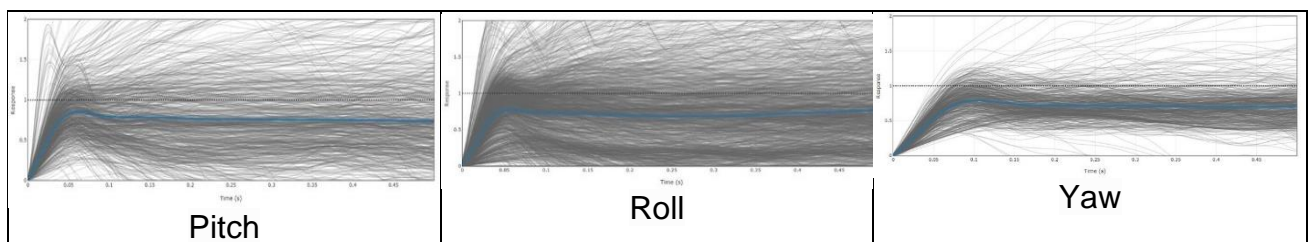
Figure 22: Step response for i) pitch ii) Roll & iii) Yaw motion

NAVIGATION SYSTEM

GPS Module helps the flight controller to find out the Geo coordinates from satellites. GPS coordinates can help in mapping the path of the flight controller for a mission.
Here 3+ GPS is a GNSS system that supports RTK mode. Positioning accuracy down to centimeter-level in an ideal environment.

Table 14:

Receiver type	u-blox high precision GNSS modules (M8P-2)
Satellite Constellation	GPS L1C/A, GLONASS L1OF, BeiDou B1I
Positioning accuracy	3D FIX: 2.5 m / RTK: 0.025 m
Processor	STM32H757
IMU sensor	ICM42688, RM3100
Navigation Update Rate	8 Hz

SELECTION OF CAMERA

The mission requirements prompted the need for a primary vision node with high resolution and sufficiently high shutter speed. Additionally, interfacing with the Herelink module required interfacing with ethernet through a DHCP query to the camera's IP address. The resolution required for the software to detect objects and identify hotspots was 20 pixels/ft.

Table 15: Comparison of specifications for various Cameras

	SIYI A2 mini	SIYI R1m	Arducam IMX 477
Dimensions	**65 x 43 x 50 mm**	42 x 42 x 25 mm	38 x 38 x 31 mm
Weight	**85 grams**	39 grams	53 grams
Resolution	**1920 x 1080p @30fps**	1920 x 1080p @30fps	4056 x 3040p @30fps 1920 x 1080p @60fps
Interface	**Ethernet**	Ethernet	CSI
Stabilization	**Single axis**	no stabilization	no stabilization
Voltage	**12v**	12v	2.8v
Focal length	**2.1mm**	3.22mm	6mm
Sensor size	**2 MP CMOS 9.407mm**	2 MP CMOS 8.758mm	12.3 MP CMOS 11.04mm
FOV	**156° (horizontal) 83.7°(vertical)**	80°(Horizontal) 57.09°(Vertical)	65°(Horizontal) 51°(Vertical)
Per pixel distance	**7.3cm (horizontal) 2.4cm(vertical)**	1.3cm(horizontal) 1.5cm (Vertical)	0.9cm (Horizontal) 1.3cm (Vertical)

The SIYI A2 mini with a 2MP CMOS sensor, was chosen for its resolution of 7.3 cm/pixel at a 15-meter altitude, offering a wide coverage of 140 meters and supporting ethernet protocol for high-speed, real-time data transmission. Its 1080p resolution ensures high-quality images necessary for hotspot identification, object detection and survey data collection. The camera features a single-axis gimbal system that maintains focus on the ROI despite variations in the drone's altitude, velocity, or vibration and a fixed yaw moment to prevent unwanted horizontal drift thus, ensuring constant horizontal alignment. To make the camera suiTable for both FPV and ground-facing orientations, the IMU controller board is mapped and controlled via SBUS wherein the signal ports are interfaced with the vehicle's autopilot. To prevent the camera from drifting into an undesired orientation, an integrated script periodically reorients the camera to maintain the correct alignment.

Figure 23: Siyi A2 mini camera

4.8. C.G. ESTIMATION & STABILITY ANALYSIS

4.8.1. C.G. ESTIMATION

Initially, our team used a manual approach to carefully arrange the components and calculate the Center of Gravity (CG) as shown in Table 16. This process involved precise measurements and calculations to determine the optimal component placement. The team then utilized SolidWorks software to virtually replicate the arrangement and simulate the CG as shown in Figure 24. This iterative process ensured a precise matching of the physical and virtual models. The nose is in negative Z direction.

Table 16: C. G. Estimation for the preliminary Design

Sr. No.	Component	Weight (kg)	D(X) (mm)	D (Y) (mm)	D (Z) (mm)	CG (x) (kgmm)	CG (y) (kgmm)	CG (z) (kgmm)
1	Frame hub	0.1	0	-43.95	-6	0	-4.395	-0.6
2	Net Rotor Arm 1	0.04	80	-39.57	-99.59	3.2	-1.5828	-3.9836
3	Net Rotor Arm 2	0.04	80	-39.57	99.59	3.2	-1.5828	3.9836
4	Net Rotor Arm 3	0.04	-80	-39.57	99.59	-3.2	-1.5828	3.9836
5	Net Rotor Arm 4	0.04	-80	-39.57	-99.59	-3.2	-1.5828	-3.9836
6	GPS with stand	0.103	0	73.31	116.57	0	7.55093	12.00671
7	Pixhawk Cube Orange with damper	0.074	0	1.5	-118	0	0.111	-8.732

| #	Component	Mass	X	Y	Z			
8	Herelink	0.09	0	-50.25	97.87	0	-4.5225	8.8083
9	Herelink antenna	0.01	-86.18	-49.2	112.43	-0.8618	-0.492	1.1243
10	Herelink antenna	0.01	86.18	-49.2	112.43	0.8618	-0.492	1.1243
11	Motor number 1	0.06	146.84	-15.1	-169.56	8.8104	-0.906	-10.1736
12	Motor number 2	0.06	146.84	-15.1	169.56	8.8104	-0.906	10.1736
13	Motor number 3	0.06	-146.84	-15.1	169.56	-8.8104	-0.906	10.1736
14	Motor number 4	0.06	-146.84	-15.1	-169.56	-8.8104	-0.906	-10.1736
15	Camera	0.085	0	-56.51	-118.74	0	-4.8033	-10.0929
16	Safety switch	0.007	1	11.5	80	0.007	0.0805	0.56
17	Buzzer	0.007	30.8	-25	67.28	0.2156	-0.175	0.47096
18	ESC	0.0025	0	-54.5	0	0	-0.13625	0
19	Landing gear 1	0.014	0	-86.83	-55.84	0	-1.21562	-0.78176
20	Landing gear 2	0.014	0	-86.83	55.84	0	-1.21562	0.78176
21	Battery	0.55	1.9	-9.5	-5	1.045	-5.225	-2.75
22	Pixhawk Power Brick Mini	0.018	0	-33.5	-95	0	-0.603	-1.71
23	Wires	0.2	0	-28.5	0	0	-5.7	0
24	Drop Mechanism	0.03	-43	-46.31	-2.5	-1.29	-1.3893	-0.075
25	Payload	0.2				0	0	0
	Total	1.9145				-0.01170018282	-17.01614521	0.07034212588
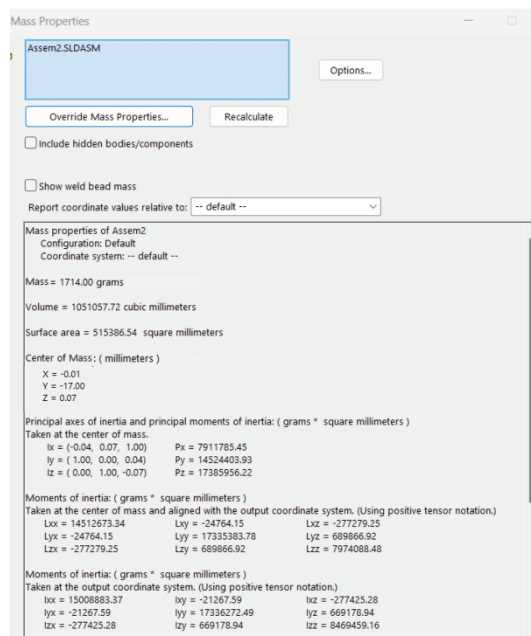
The Manual moment calculation is attached as
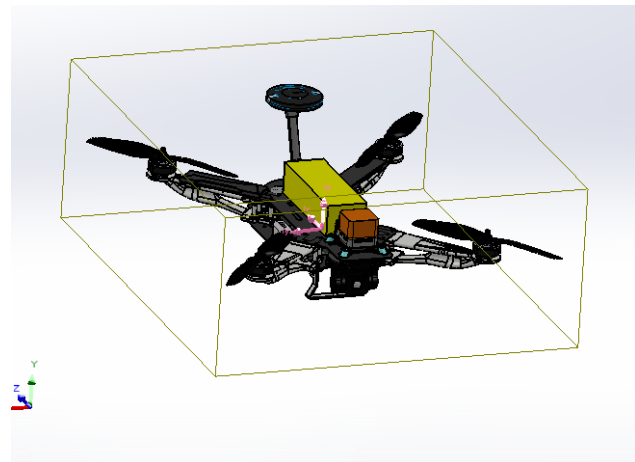
Figure 24: i) Mass property & ii) C.G. of UAS from SolidWorks

4.8.2. STABILITY ANALYSIS

MECHANICAL STABILITY OF UAS

Several critical factors affect stability of UAS, including motor-to-motor distance, mass distribution, and thrust line of UAS.

MOTOR-TO-MOTOR DISTANCE (ALONG PITCH VS. ALONG ROLL)

-In UAS configuration, the horizontal motor-to-motor distance is shorter compared to the vertical motor-to-motor distance. This design inherently provides greater stability along the roll axis.

- The increased stability in the roll axis results from the shorter horizontal span, which reduces the lever arm effect and thus minimizes rotational inertia around the roll axis. Consequently, UAS exhibit enhanced roll stability, making them more resilient to disturbances like wind guests.

MASS DISTRIBUTION (PITCH AXIS MOUNTING SCHEME

- Concentrated mounting scheme along pitch axis of UAS results in a higher moment of inertia around the pitch axis compared to the roll axis as shown in Figure 24.

-Due to the higher moment of inertia and maneuverability in the pitch axis, UAS can achieve higher speeds with a lower angle of attack. This capability is crucial for missions requiring sustained forward movement.

-The ability to maintain higher speeds with a minimal angle of attack reduces aerodynamic drag and improves propulsion efficiency. As a result, the UAS can achieve greater endurance, making it suiTable for long-duration missions where sustained forward motion is critical.

ELECTRICAL STABILITY

For getting sTable PID in tuning process, set up notch filter and temperature calibration before tuning and after tuning, barometer compensation is mandatory. Stability depends upon these two setups process which are as of below.

1. Notch filter

• There are two ways to damp vibrations in drone I) Mechanical Shock Absorber (Damper) II) Use of Digital Filter

• Notch filter is a band stop filter which attenuates the natural frequency of motor using band stop filter.

• In order to set up of Notch filter we have plotted time domain log of flight into frequency domain using Fast Fourier Transform (FFT) above Nyquist criteria which results in graph shown in Figure 25,
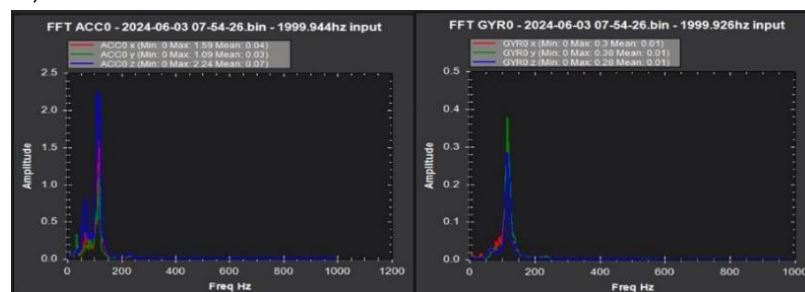

Figure 25: FFT graph before filtering

This shows drone has maximum vibration frequency amplitude at 112 Hz, so in order to attenuate it notch filter is set up at 112 Hz with bandwidth of 56 Hz, which results in below post flight analysis graph shown in Figure 26, which shows successful attenuation of peak amplitude at different
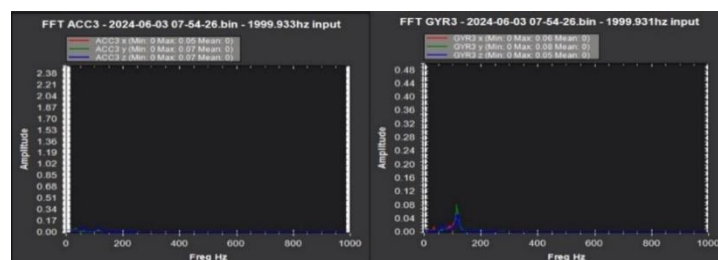
Figure 26: FFT graph after filtering

2. Temperature Calibration

- Calibrating the IMU for temperature changes can greatly reduce the amount of variation in the IMU and helps with flying in conditions where the temperature varies a lot between bootup and flight.
- In order to do temperature calibration, we have to set up temperature learning parameters of flight controller and then cool the flight controller below the minimum operating temperature.
- Then ensuring no movement during the calibration process, resulting in the flight controller acquiring the values for compensating temperature change.
- Now, flight controller is ready to give sTable response with variation in temperature.

3. Windspeed estimation and Barometer compensation

- Flight controllers EKF can estimate the windspeed flying without requiring an airspeed sensor. This can be useful information to compensate for wind related barometer interference.
- We have calculated frontal area and side area by using 3D CAD model of drone.
- After establishing windspeed we calculated
- EK3_DRAG_BCOEF_X = mass in kg / frontal area in m^2
- EK3_DRAG_BCOEF_Y = mass in kg / side area in m^2

Then we have calculated value of momentum drag using above parameters and graph. Once it is enabled, it can be used to compensate for the wind's effect on each barometer in each of four directions (forward, back, left, right).
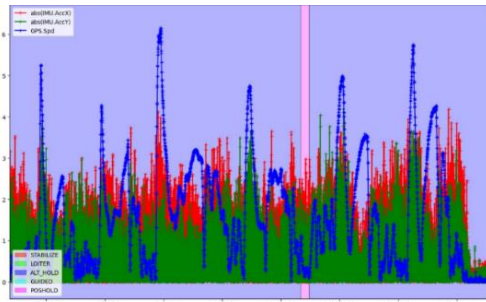
Figure 27: Graph for wind speed estimation

CAD MODEL OF PRELIMINARY DESIGN
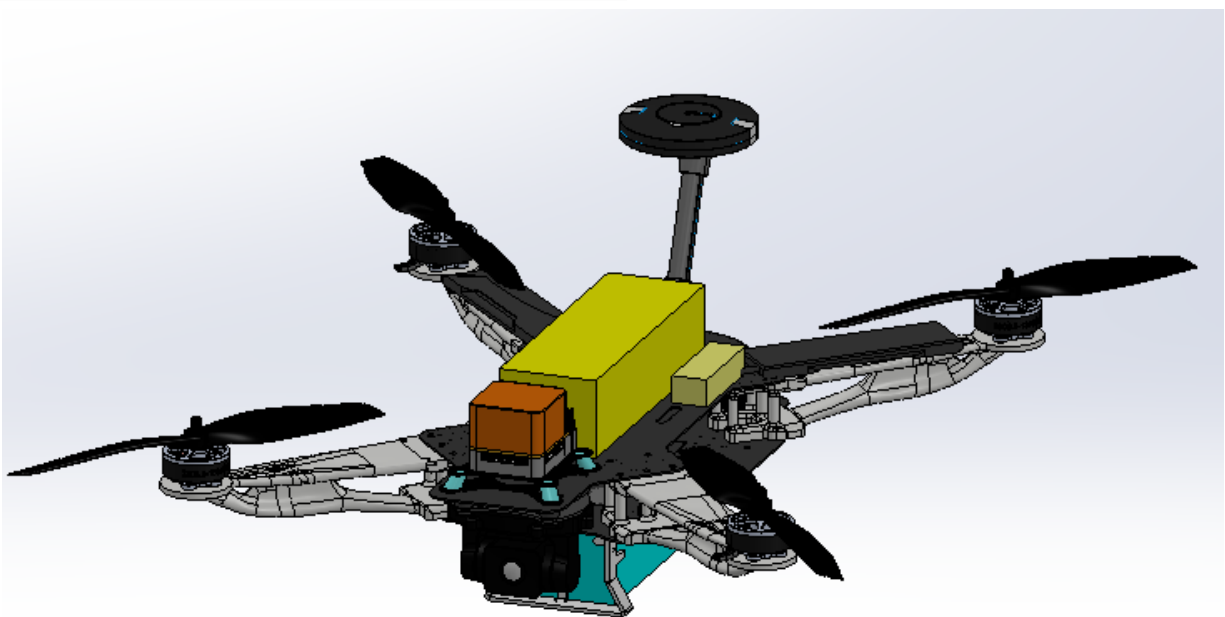
Figure 28: CAD model of Preliminary design

4.9. DETAILED DRAWING

The detailed drawing of the initial design of an UAS is as shown below.

Item No.	Part Name	Description	Quantity
1	Pixhawk	Pixhawk Cube Orange	1
2	Battery	Genx PRO 6750 mAH(4s)	1
3	Linear Actuator	Payload Dropping Mechanism	1
4	Buzzer	buzzer	1
5	Motor	Xing 2806.5 1300 kv	4
6	Motor Arms	CFRP arms	4
7	Propeller	8*4.5"	4
8	ESC	4 in 1 ESC T motor F55	1
9	Herelink	Air Unit	1
10	Herelink Antenna	Transmission	2
11	GPS	Here 3+	1
12	GPS Stand	stand for here 3+	1
13	Landing Gear	Aluminium bended landing gear	2
14	Camera	Siyi a2 mini	1
15	Payload	payload	1
16	Top Plate	top plate	1
17	Bottom Plate	bottom plate	1
18	Power Brick	Pixhawk power brick mini	1
19	Safety Switch	hardware safety for accidental arming	1

UNLESS OTHERWISE SPECIFIED DIMENSIONS ARE IN MILLIMETERS

CG Information From Datum		Summary Data		Institute of Technology Nirma University
Datums	A, B and C are in same datum	WHEELBASE	448.71	AEROTHON 49
		EMPTY WEIGHT:	1.2 kg	
		MOTOR	Xing x2806.5 1300kv	PRELIMINARY DESGIN
		PROPELLER	8x4.5	A3

SCALE:1:5   SHEET 1 OF 2

4.10 COMPUTATIONAL ANALYSIS

At this stage it was necessary to validate the readiness of a system. To achieve this, we employed a multi-faceted approach. Firstly, static structural analysis was conducted to assess the strength and durability of components. Next, modal analysis was performed to determine the natural frequency of the system. Explicit dynamic analysis was also utilized to simulate impact scenarios, while computational fluid dynamics (CFD) was used to study fluid flow, thrust loss, and drag estimation. Furthermore, our team leveraged generative design and shape optimization techniques to optimize the design for the best possible outcome. To accomplish this, we seamlessly integrated Fusion 360 and Ansys software tools.

4.10.1. GENERATIVE DESIGN OF ROTOR ARM

As mentioned previously, for rotor arm we opted for the generative design, for this purpose we choose the fusion 360 software's generative design feature. To generate a design, we must provide specific parameters, including,

- − Load cases, which define the forces and fixtures applied
- − Material types that can be utilized
- − Targeted factor of safety and component mass
- − Preferred manufacturing process

A rough design outline, which includes:
- o Preserve bodies (Green)
- o Starting shapes (Yellow)
- o Obstacle bodies (Red)

By providing these parameters, we created an optimized design that meets the desired performance, factor of safety, and manufacturing requirements.

Preliminary rotor arm: Initially we opted for factor of safety as 3 & weight of 30 grams over the given load conditions.

Load Cases	Magnitude	Direction (x, y, z)
1	30N	0,1,0
2	30N	0.6,1,0
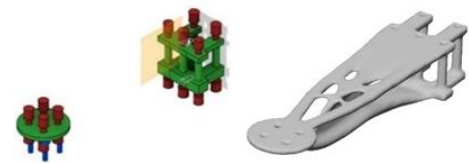
Figure 29:

Final rotor arm: Initial flight testing and CFD analysis showed that the preliminary design's large cross-sectional area resulted in substantial thrust loss and a high drag coefficient. To mitigate this, we incorporated an obstacle geometry that limited the arm's thickness, achieving enhanced flight time, reduced thrust loss, and improved performance. The final design's parameters and post-processing procedures remain consistent with the preliminary design, with the added optimization.
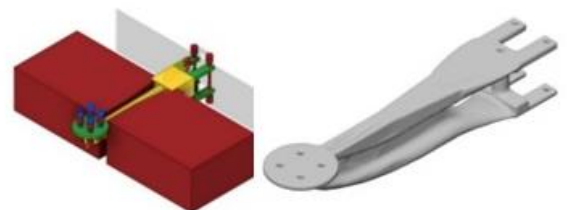
Figure 30:

Table 17: Results for preliminary & Final rotor arm design

Parameters	Expected	Preliminary Results	Final Results
Factor of safety	3	3	3.05
Mass	30 grams	30 grams	27 grams

4.10.2. FINITE ELEMENT ANALYSIS

STATIC STRUCTURE

A comprehensive structural analysis was performed utilizing finite element analysis (FEA). Initially, we calculated the individual stresses and deformations of critical components, such as rotary arms and plates. Subsequently, we estimated the cumulative stress and

deformation experienced by the entire system under various loading conditions, simulating real-life scenarios that our UAS may encounter in operation. This rigorous analysis enabled us to evaluate the system's structural integrity and performance under diverse loads.

FEA OF ROTOR ARMS

As the raw generated design may not perform optimally under various real-life scenarios and potential printing errors, we refined the design to enhance its overall performance.

Figure 31: FEA of rotor arm

Table 18: Comparison of various performance parameters of preliminary & final design

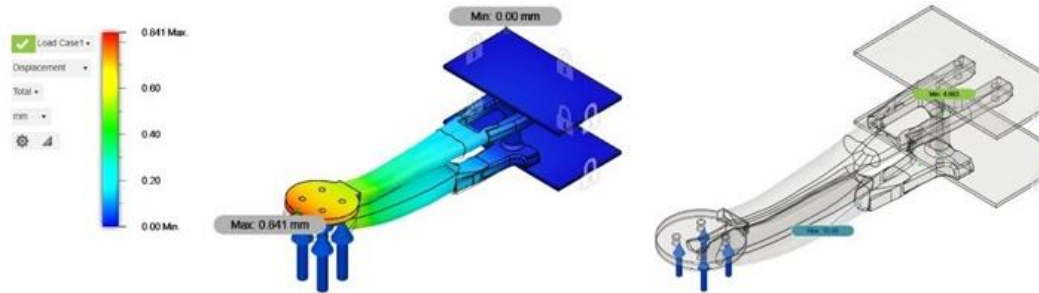|	Preliminary Design	Final Design
Factor of Safety	4.2	3.7
Deformation	0.5 mm	0.8 mm
Stress	4.9 MPa	5.3
Weight	40 grams	34 grams

FEA OF LANDING GEAR
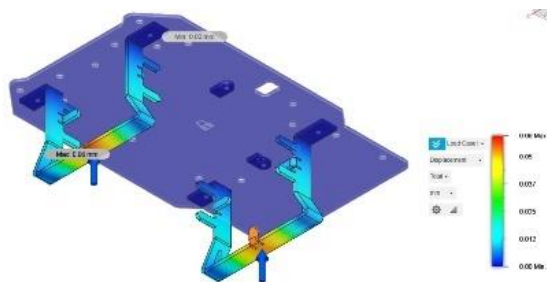
Figure 32: FEA of landing gear

We simulated the static conditions that the landing gear may encounter. For static analysis we opted to simulate under 5 times the actual load i.e. 100 N approximately, vertically and also at the edges. Results are mentioned as shown in Table

Table 19: Comparison of preliminary & final landing gear

Parameters	Preliminary	Final
Factor of safety	2.65	3.23
Deformation	0.1mm	0.06mm
Stress	53MPa	35 Mia

By this result would conclude that our landing gear can support and prevent togging of UAS

FEA OF UAS UNDER VARIOUS CONDITIONS:
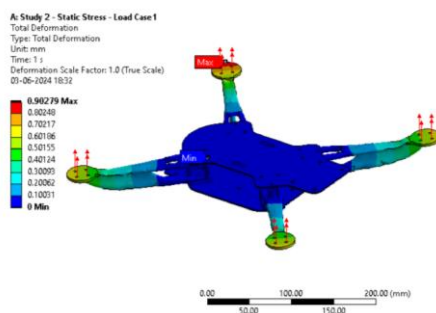
Figure 33: FEA of UAS

We simulated real-life scenarios, including combined pitch and roll moments, yaw moment, and harsh landing conditions, to ensure the UAS's structural integrity and performance under diverse loads. We got minimum FOS of 3.5 and maximum deformation of 0.9 mm, thus validating our design.

MODAL ANALYSIS

This analysis aimed to determine the natural frequencies of our Unmanned Aerial System (UAS) to avoid resonant conditions. Resonance can occur when the motor's vibrational excitations transfer to the body, potentially causing deformation.

We calculated the vibrational excitations using the formula: $v = \frac{RPM}{60}$ for maximum angular velocity which is 21840 RPM the maximum frequency is 364

Our results (Figure 34 (ii)) showed that the first harmonic frequency 81.789 does not match the natural frequencies obtained from modal analysis, indicating no risk of deformation due to resonance phenomena.

Figure 34: i) Modal Analysis of UAS & ii) Frequency at various modes

EXPLICIT DYNAMICS

This type of nonlinear analysis enables us to simulate the impact of a crash on our drone and estimate the potential damage to our system. By utilizing this analysis, we can gain valuable insights into the effects of crash loads on our drone's structural integrity and predict the extent of damage that may occur. By explicit dynamics it was concluded that the all the electronics component, frame hub & rotor arms are safe even in case fall, landing gear may break down, that has max stress of 329.4 MPa.
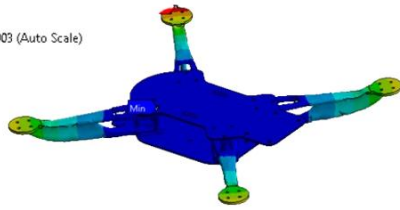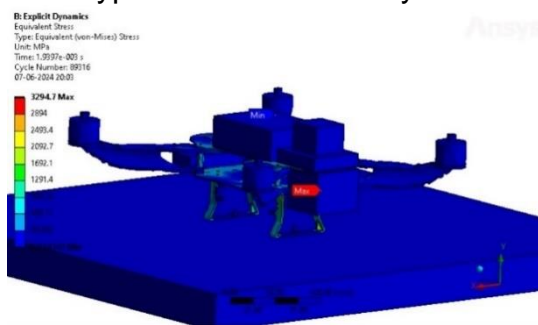
Figure 35: Explicit dynamics of UAS

4.10.3. CFD

We employed transient CFD simulations to investigate the aerodynamic characteristics of our UAS, analyzing the transient behavior of physical variables pertaining to aerodynamic performance. The simulation encompassed:

- Propeller clearance analysis to ensure minimal interference
- Full-body CFD analysis to detect potential vortex formation and interference with the main body
- Drag coefficient calculation to optimize aerodynamic efficiency

Table 20: Parameters for propeller & full body CFD

Parameters	Propellers	Full Body
Model Used	k-Omega	k-epsilon
Mesh Metric (Orthogonal)	0.1	0.1
Condition	Transient	Steady state
Solver type	Pressure Based	Pressure Based
Density of Air	1.225 kg/m^3	1.225 kg/m^3
Inlet Velocity	0 m/s	0 m/s
RPM of propeller	21,000	21,000
Outlet pressure (gauge pressure)	0 Pa	0 Pa
Residuals	1.0 x 10E-4	1.0 x 10E-4
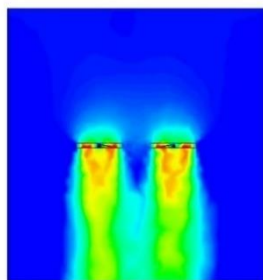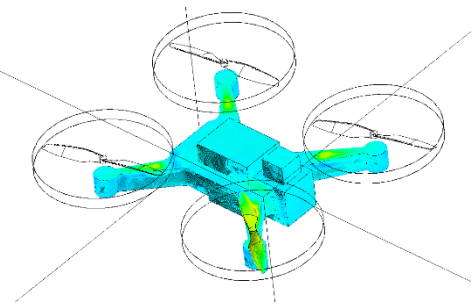
Figure 36: i) CFD of propeller ii) Full body CFD

Result for Propeller CFD		Result for full body CFD
Lift	22.8 N	21.3 N

From the insights to pressure contour, velocity & streamlines it was concluded that some amount thrust lost was experienced yet the UAS was capable enough to survive the same. CFD analysis yielded crucial insights into the UAS's aerodynamic behavior, allowing us to optimize our design for better aerodynamic performance

4.11 OPTIMIZED FINAL DESIGN

Initially, the team utilized a standard Li-Po 6200 mAh battery, but through innovative design and engineering, we successfully developed a customized 6750 mAh solid-state battery. This upgrade resulted in significant improvements, including:

- Weight reduction

- Enhanced endurance

- Compact battery design

The compact battery design, in turn, enabled a reduction in the frame hub's dimensions, leading to further weight savings. Notably, the new frame design achieved an optimal aspect ratio of 2.2, ideal for surveillance drones. The Table 21 below summarizes the comprehensive design enhancements made to the initial prototype

Table 21 Summary of the changes made in the frame

	Initial	Final
Dimensions of the top plate	273.20 x 136.91 mm^2	235.27 x 104.66 mm^2
Dimensions of the bottom plate	225.62 x 136.91 mm^2	184.23 x 112.91 mm^2
Motor-to-Motor Distance (1)	339.8 mm	300 mm
Motor-to-Motor Distance (2)	292.88 mm	280 mm
Wheelbase	448.72 mm	410.37 mm
Battery	Li-PO 6200 mAh	Solid State 6750 mAh

1. Along Pitch, 2. Along Roll

4.11.1. FINAL CAD MODEL
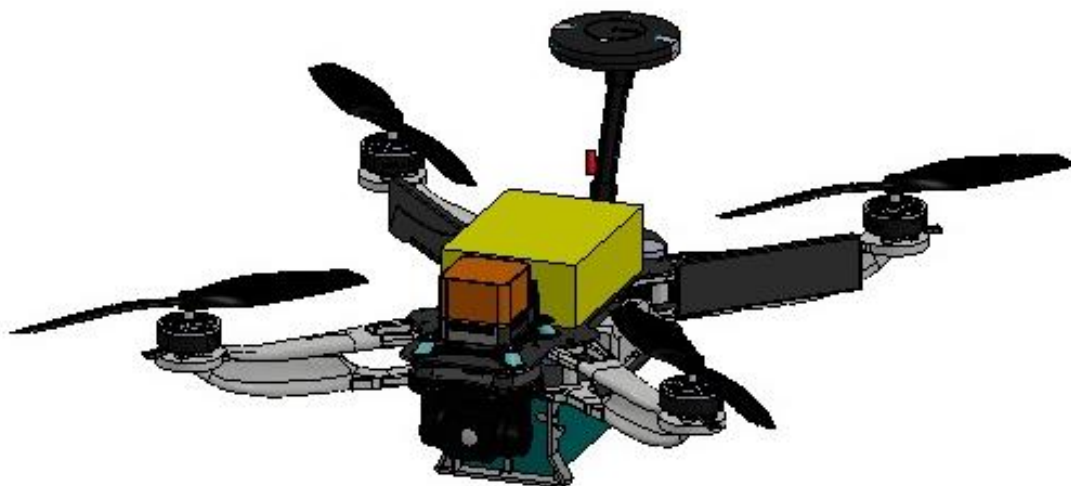
Figure 36: CAD model for final Design

4.11.2. 2D DRAFTING & C.G

Item No.	Part Name	Description	Quantity
1	Pixhawk	Pixhawk Cube Orange	1
2	Battery	Genx PRO 6750 mAH(4s)	1
3	Linear Actuator	Payload Dropping Mechanism	1
4	Buzzer	buzzer	1
5	Motor	Xing 2806.5 1300 kv	4
6	Motor Arms	CFRP arms	4
7	Propeller	8*4.5"	4
8	ESC	4 in1 ESC T motor F55	1
9	Herelink	Air Unit	1
10	Herelink Antenna	Transmission	2
11	GPS	Here 3+	1
12	GPS Stand	stand for here 3+	1
13	Landing Gear	Aluminium bended landing gear	2
14	Camera	Siyi a2 mini	1
15	Payload	payload	1
16	Top Plate	top plate	1
17	Bottom Plate	bottom plate	1
18	Power Brick	Pixhawk power brick mini	1
19	Safety switch	hardware safety for accidental arming	1

UNLESS SPECIFIED DIMENSIONS ARE IN MILLIMETERS

CG Information From Datum		Summary Data		Institute of Technology Nirma University
Fwd CG (x,y,z)	-0.45,-14.91,46.08	LBH	300x280x193	
AFT CG (x,y,z)	-0.45,-14.91,-44.58	EMPTY WEIGHT:	1.160	AEROTHON 49
Empty CG	-0.45,-14.91,1.03	MOTOR	Xing x2806.5 1300kv	
Datums	A,B and C are in same datum	PROPELLER	8x4.5	FINAL DESGIN

SCALE:1:5   SHEET 2 OF 2   A3

4.12. DETAILED WEIGHT BREAKDOWN & C.G. OF FINAL UAS DESIGN

The final weight breakdown of the Unmanned Aerial System (UAS) was extracted from the finalized Computer-Aided Design (CAD) model. The mass properties of the system, as analyzed by SolidWorks 2022, are presented in the Figure 37. Additionally, a manual calculation of the Center of Gravity (C.G.) was performed, and the results are summarized in the Table 9 below, providing a comprehensive understanding of the system's mass distribution and balance.
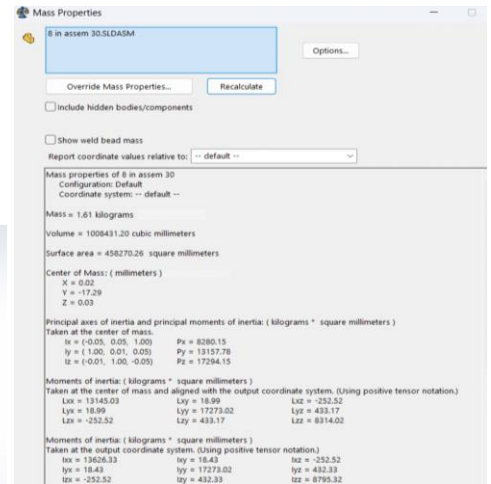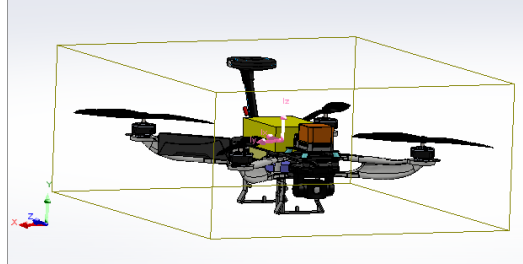

Figure 37: Final Design mass property & C.G. from solid works.

Table 22: Detailed weight breakdown & C.G. estimation.

Sr. No.	Component	Weight (kg)	D(X) (mm)	D (Y) (mm)	D (Z) (mm)	CG(x) (Kg-mm)	CG (y) (Kg-mm)	CG (z) (Kg-mm)
1	Frame hub	0.087	0	-43.95	6	0	-3.82365	0.522
2	Net rotor arm 1	0.038	80	-39.57	-99.59	3.04	-1.50366	-3.78442
3	Net rotor arm 2	0.038	80	-39.57	99.59	3.04	-1.50366	3.78442
4	Net rotor arm 3	0.038	-80	-39.57	99.59	-3.04	-1.50366	3.78442
5	Net rotor arm 4	0.038	-80	-39.57	-99.59	-3.04	-1.50366	-3.78442
6	GPS with stand	0.1	0	73.31	80.84	0	7.331	8.084
7	Pixhawk Cube Orange with damper	0.074	0	1.5	-99.6	0	0.111	-7.3704
8	Herelink	0.09	0	-50.25	95.62	0	-4.5225	8.6058
9	Herelink antenna	0.01	100	-49.2	100.82	1	-0.492	1.0082
10	Herelink antenna	0.01	-100	-49.2	100.82	-1	-0.492	1.0082
11	Motor number 1	0.0613	140.3	-15.1	-150.24	8.60039	-0.92563	-9.209712
12	Motor number 2	0.0613	140.3	-15.1	150.24	8.60039	-0.92563	9.209712
13	Motor number 3	0.0613	-140.3	-15.1	150.24	-8.60039	-0.92563	9.209712
14	Motor number 4	0.0613	-140.3	-15.1	-150.24	-8.60039	-0.92563	-9.209712
15	Camera	0.085	0	-56.51	-97.65	0	-4.80335	-8.30025
16	Safety switch	0.007	1	11.5	80	0.007	0.0805	0.56
17	Buzzer	0.007	30.4	-25	67.28	0.2128	-0.175	0.47096
18	Esc	0.0025	0	-54.5	0	0	-0.13625	0
19	Landin gear 1	0.014	0	-86.83	-55.84	0	-1.21562	-0.78176
20	Landing gear 2	0.014	0	-86.83	55.84	0	-1.21562	0.78176
21	Battery	0.45	2	-9.5	-4.027	0.9	-4.275	-1.81215
22	Pixhawk power brick mini	0.028	0	-33.5	-95	0	-0.938	-2.66
23	Wires	0.2	0	-28.5	0	0	-5.7	0
24	Drop mechanism	0.025	-43	-46.31	-2.5	-1.075	-1.15775	-0.0625
25	Payload	0.2				0	0	0
	Total	1.8007				0.02487 921364	-17.29405231	0.029910 59033

The moment calculation for the same is attached as <u>reference 9</u>

4.13. UAS PERFORMANCE RECALCULATION (THRUST/WEIGHT, POWER REQUIRED FOR THE MISSION & ENDURANCE CALCULATION)

Due to change in the weight of the UAS; there would be change in the values of the Thrust and the power. Therefore, recalculation of the power and thrust was done.

THRUST CALCULATION

As the final weight of UAS is 1.8kg & the practical thrust calculated by thrust bench test is 2kg at 100% throttle & at 70% throttle the thrust is 1.3kg

Thus, calculating thrust to weight at cruise condition,

$$\frac{Thrust}{Weight} = \frac{1.3 * 4}{1.8} = 2.88$$

POWER CALCULATION

For smooth functioning of an UAS mission, 60%-70% throttle is required which draws 30 A of current. As battery is 4 cells, voltage is 16V

$Power\ required = Voltage * Current = 16 * 30 = 480W,$

Hence, total power required for mission is 480 + 30 = 510W

* 30W is for auxiliary electronics.

ENDURANCE CALCULATION

Based on new Battery, the endurance is calculated as: $Endurance = \frac{Watt-h*60}{Total\ Watt}$

$Watt\ hour\ rating = No.of\ cell * nominal\ volatge * battery\ capacity = 4 * 3.7 * 6.75 = 99.99\ Wh$

Thus, based on watt hour rating and power consumption estimation the estimated endurance is

$$Endurance = \frac{99.99 * 60}{510} = 11.8 min$$

5. FINAL UAS SPECIFICATIONS AND BILL OF MATERIALS

FINAL UAS SPECIFICATION

Table 22: Final UAS specification

Specification	Measurement
Final weight	1.8Kg (Including Payload)
Empty Weight	1.15kg (Frame weight)
Thrust/ Weight	3.2
Maximum speed	9m/s
Endurance	11.8 mins
Maximum Dimensions (L*W*H)	300*280*193.47
Maximum angular speed	21840 RPM
KV ratings	1300
Propeller Size	8*4.5 inches
Wheel base	410.37mm
Communication range	2KMs
Total thrust	5.2 Kg-f

BILL OF MATERIALS

<div align="center">Table 23: Bill of Material</div>

Sr. No.	Component	Quantity	Material
1	Top Plate	1	CFRP
2	Bottom Plate	1	CFRP
3	Arms	4	PET-G infused with 15% CF
4	Bolts	41	Stainless Steel
5	Landing Gear	2	Aluminum
6	GPS Stand	1	CFRP
7	Pixhawk Cube Orange	1	
8	Herelink	1	
9	Herelink Antenna	2	
10	Motors	4	
11	Propeller	4	CFRP
12	Camera	1	
13	GPS	1	
14	Buzzer & Safety Switch	1	
15	ESC	1	
16	Battery	1	
17	UBEC	2	
18	Wires	-	
19	Drop Mechanism	1	
20	Payload	1	Plastic
Total		77	

The Cost estimation for the same is attached as Reference 10

6. SYSTEM DESIGN FOR CAPTURING THE SURVEY DATA

6.1. CAPTURING THE SURVEY DATA

Actual Distance

$$\text{Actual Distance}_{x\,axis} = \text{No. of Pixels} * \left(\frac{2*h*\tan\theta_x}{\text{Image width}}\right)$$

$$\text{Actual Distance}_{y\,axis} = \text{No. of Pixels} * \left(\frac{2*h*\tan\theta_y}{\text{Image height}}\right)$$
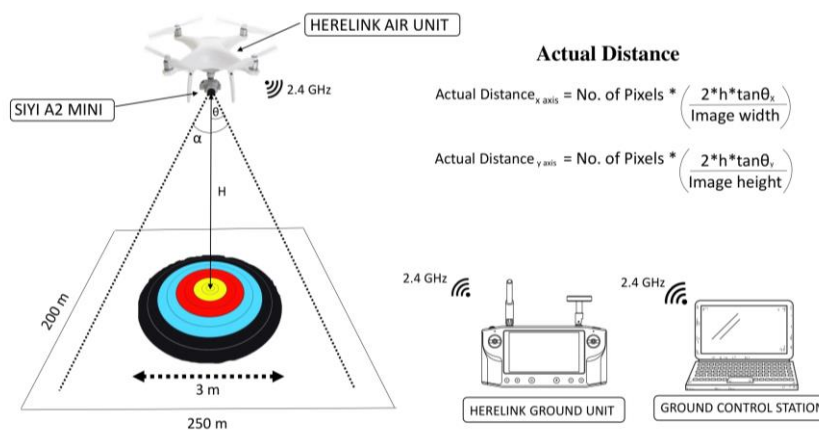
Figure 38: Video transmission & FOV of camera

The system design for capturing survey data is built around a camera stabilized by a motorized gimbal. As the UAS traverses the survey grid, the vision node captures real-time images. The imaging system manages image capture, resizing the images to 1080p, which are subsequently transmitted as RTP packets using RTSP. The wider FOV covers blind spots in the survey field, maximizing coverage with minimal resource usage and overlapping images to avoid false detections and ensure redundancy.

The camera interfaces with the Herelink air unit, utilizing the Ethernet protocol for transmitting survey data. A script running on the ground computer periodically adjusts the gimbal orientation. For parallel communication, the transmission protocol employs TCP tunnelling to multiplex RTSP stream transfer and serial communication with the IMU gimbal controller board. Frames are encoded using H.265 and transmitted via the 2.4GHz Wi-Fi band to the Herelink ground unit, which then locally transmits the data to the ground computing unit. The data is decoded and processed for geotagging.

An integrated script queues the detected and geotagged hotspots, tagging each image with an NTP timestamp. These parameters are converted into JSON packets, which are made available for retrieval on both the local computer and a server for redundancy.

7. METHODOLOGY FOR AUTONOMOUS OPERATIONS

7.1 AUTONOMOUS FLIGHT:

The Ground control station or the GCS used, in the team's case would be mission planner which would read the waypoints provided by the team which would be forming an entire grid-like pattern to search for the payload, autonomously maneuvering in a particular area. The UAS will be fed the path through the Pixhawk Orange via the telemetry. The UAS will search the entire area for the required target and hotspots for which the flight controller and ground computer is connected. On detecting a hotspot, the UAS will autonomously geotag the coordinate to avoid overlap and enable retrieval. Upon entering the search grid, the coordinates of the GPS are given to the computer via the Pixhawk and in return, it will give out instructions to navigate to identified coordinates. It is further required to identify the target, after detecting all the hotspots, and thus descend to an altitude of 5 m, and perform the payload drop. On competition of the task, the UAS will be provided a mission command, 'RTL', enabling the copter to autonomously return to the take-off position. The issue of telemetry loss Ground computing being potential threat of loss of communication between the flight controller and the ground computer was resolved by embedding a Lua script in the flight controller which pings the IP of ground computer continuously. Upon loss of packets, the script would change the current mode from 'GUIDED' back to 'AUTO' and execute the last waypoint provided by the flight controller. Concurrent communication loss exceeding a threshold time would result in 'RTL' of the UAS.

7.2. TARGET IDENTIFICATION:

Upon entering the search grid, the drone transitions from 'AUTO' mode to 'GUIDED' mode. To maximize field coverage and minimize flight time, the area coverage of the camera was calculated and the grid was divided into 16 midpoints based on the dimensions as shown in Figure 39. The ground computer mirrors the telemetry stream and sends MAVlink packets to traverse the UAS to the identified midpoints. To counter GPS

Figure 39 Field griding of the search area

inaccuracy leading to overlapping images, the coordinates of the detected objects are hashed in a vector pair and compared with the coordinates of the new object. Hash map counting would only be increased once unique coordinates are accumulated.
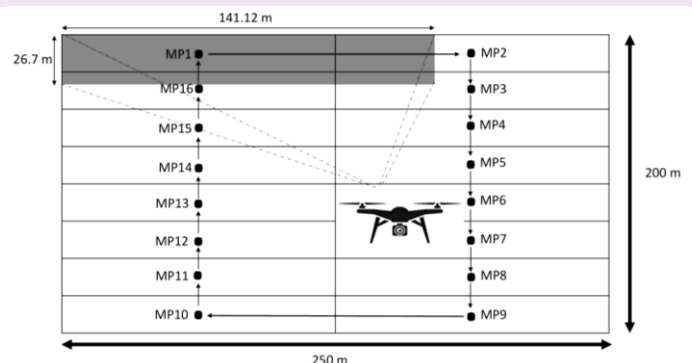
A script running on the ground computer leads the UAS to the identified coordinates and initiates an algorithm hereby. Main goal of the algorithm was to autonomously detect region of interest (ROI) then identify the shape and map the detected class with its frequency along with the lowest memory consumption, highest possible speed and accuracy. The algorithm is implemented using the OpenCV library in Python, prioritizing computer vision techniques over neural network algorithms. The image taken from the camera is transferred to the local computer. The processing involves smoothening of the image followed by a canny edge algorithm. Contours of the image are extracted and used to eliminate irrelevant contours to detect ROI. To detect shape in the ROI, it is grayscale and threshold using adaptive and OTSU thresholding. Weights are assigned to the resulting images, and the class with the most threshold is assigned to the image. Reference 11
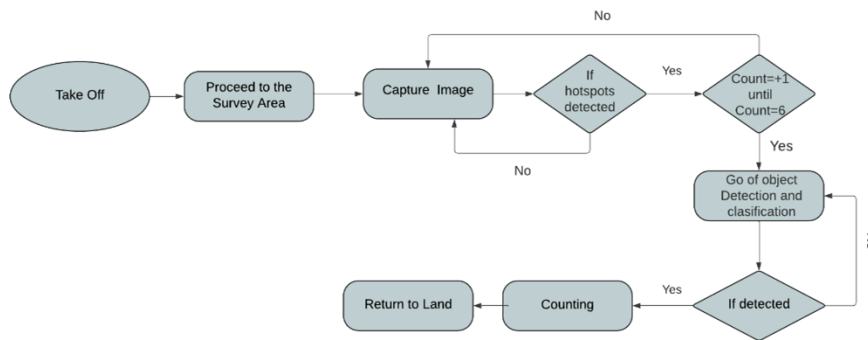
Figure 40: Outline of steps to achieve mission 2

Identification of hotspots and target was formulated using a novel ODLC pipeline based around YOLO-V5x6, additional SPP module and PANet aggregation at the neck complementing the top-down pathway by adding a bottom-up path. This approach required a dataset to train our model, hence prompting the need to synthetically create a dataset. To improve the object detector's accuracy, we proceeded with data augmentation of previous years background images of the field of the competition and were able to combine 1 images of the training dataset to 5 images, greatly reducing the need of selecting a large mini-batch size for training.

The algorithm is initiated when the drone is airborne. Upon detection of a hotspot the drone transitions from its current mode to guided mode, transferring its control to the ground computer, mirroring the telemetry stream from the flight controller. The drone is commanded according to the output from the model and other calculations to navigate towards the said geocoordinate. Each detected hotspot is geotagged, and the ADC timestamp is recorded by a script that queues the camera serially, correlating it with the point of throttle increase. These parameters are then converted to a JSON packet and are available for retrieval on the local computer as well as server for redundancy.
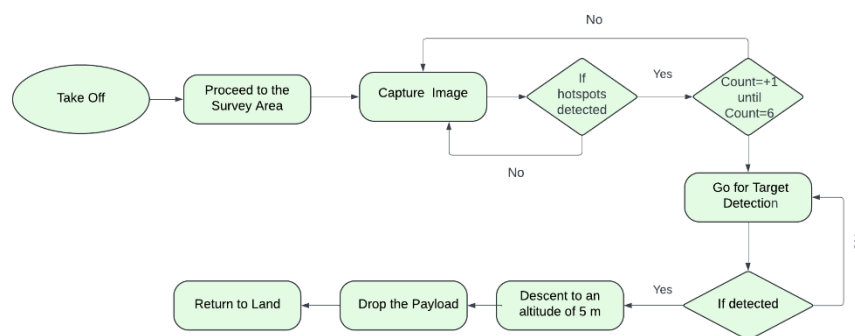

Figure 41: Outline of steps to achieve mission 3

Upon successful identification of the target, the drone transitions its mode from 'AUTO' to 'GUIDED' and is commanded using the outputs of the model. The drone navigates to the said geocoordinate and descends to a height of 5m to proceed with the payload dropping mechanism.

7.3. PAYLOAD DROP:

PAYLOAD

- Dimension: 10*5*5 cm
- Material: Plastic
- Weight: 200gms
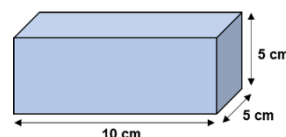
SETUP & MECHANISM
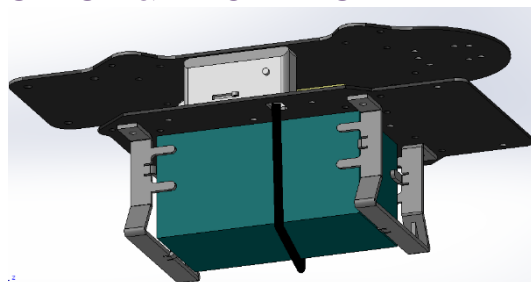
Figure 42: Payload dropping setup

The payload drop mechanism consisted of a linear actuator, along with a nylon strap. The payload is enclosed in stopper plates, held by the nylon strap. Manually, it is actuated using the RC Transmitter, which is set up by mapping the channel of the transmitter, using the logical switches, with the GCS.

Mechanism: Upon detection of the object by the camera, a signal is instantly sent to the ground

station. Following manual confirmation, the PWM signal is adjusted, changing from a high of 1900 microseconds to a low of 1100 microseconds, thereby actuating the linear actuator and releasing the payload within 0.4 seconds.

8. SUMMARY & INNOVATION

The team successfully designed, developed, and integrated an Uncrewed Aerial System (UAS) that fully complied with the mission requirements and rules of the Aerothon competition. The compact and lightweight UAS has a total mass of less than 2kg, achieved an endurance of approximately 12 minutes & optimization of the aircraft's aerodynamic design & power systems.

Utilizing advanced computer-aided design (CAD) software, specifically the generative design feature of Fusion 360, the team optimized the rotor arm for enhanced structural integrity, and weight reduction.

Integrated landing gear design that consolidates functionality, reducing weight and enhancing structural reliability. This innovative approach enabled the consolidation of functionality, resulting in a robust and efficient landing gear system.

The team also designed and developed a custom-built battery, carefully optimized for weight and energy density, to maximize endurance and meet the demanding mission requirements. Additionally, a camera-based object detection system was integrated into the UAS, providing advanced detection and tracking capabilities.

The UAS features a rapid-release dropping mechanism, deploying within 0.4 seconds of detection, made possible by a sophisticated "smart" design that combines object detection, manual confirmation, and precise PWM signal control. This innovative system ensures accurate and rapid release, showcasing the team's exceptional engineering expertise and problem-solving skills.

9. PROOF OF FLIGHT

Proof of flight consist of demonstration on an UAS build by Team arrow for Aerothon 2024.

https://drive.google.com/file/d/1Iwxtn1whKoUmUJ4kkOGX7sTgT4sgFXml/view?usp=sharing

10. BIBILOGRAPHY

- FPV drone with GPS used for surveillance in remote areas INSPEC Accession Number: 17467625
- Z. Zaheer, A. Usmani, E. Khan and M. A. Qadeer, "Aerial surveillance system using UAS", 2016 Thirteenth International Conference on Wireless and Optical Communications Networks (WOCN), pp. 1-7, 2016.
- E. Wang, S. Zhang and Z. Zhang, "Research on Composite Material UAS Low-Cost Avionics System Prototype", 2012 8th International Conference on Wireless Communications Networking and Mobile Computing, pp. 1-4, 2012.
- V. Mhatre, S. Chavan, A. Samuel, A. Patil, A. Chittimilla and N. Kumar, "Embedded video processing and data acquisition for unmanned aerial vehicle", 2015 International Conference on Computers Communications and Systems (ICCCS), pp. 141-145, 2015.
- Flying Into the Wind: Insects and Bio-Inspired Micro-Air-Vehicles with a Wing-Stroke Dihedral Steer Passively into Wind-Gust.

- Mellinger, D., Michael, N., Kumar, V.: Trajectory generation and control for precise aggressive maneuvers with quadrotors. In: Proceedings of the International Symposium on Experimental Robotics (2010)
- Bouabdallah, S.: design and control of quadrotors with application to autonomous flying. PhD thesis, EPFL (2007)
- Optimization of Propeller Performance for a Quadcopter Drone by Applying Aerodynamic Propeller-Ducts
  Part of the Lecture Notes in Networks and Systems book series (LNNS, volume410)
- Ohanian, K.O.J., Gelhausen, P.: Ducted Fan UAS Modeling and Simulation in Preliminary Design, AVID LLC (2007)
- Journal of Xi'an University of Architecture & Technology SURVEY PAPER ON DRONES CHARACTERISTICS ISSN No: 1006-7930 •
- Journal of Civil & Environmental Engineering
- Overview of Propulsion Systems for Unmanned Aerial Vehicles
- Unmanned aerial vehicles optimal airtime estimation for energy aware deployment in IoT-enabled fifth generation cellular networks
- Flight Time Estimation for Continuous Surveillance Missions Using a Multirotor UAS Sunghun Jung 1, Yonghyeon Jo and Young-Joon Kim
- International Research Journal of Engineering and Technology (IRJET) Selection of BLDC Motor and Propeller for Autonomous Amphibious Unmanned Aerial Vehicle

REFERENCE

REFERENCE 1

Detail for drone configuration.

https://discuss.ardupilot.org/t/building-a-better-quad-frame/27703/8

REFERENCE 2

Comparison of propeller with various number of blades.

https://hartzellprop.com/are-more-propeller-blades-better/#:~:text=A%202%2Dblade%20propeller%20produces,inherently%20smoother%20and%20therefore%20quieter.

REFERENCE 3

Comparison of various 3D printing methods.

Method Properties	FDM	MJF	Sla
Accuracy	Moderate	Moderate	High
Surface Finish	Least	Moderate	High
Availability	Maximum	Moderate	Moderate
Ease of USE	Moderate	Maximum	Moderate
Cost	Least	Moderate	High

REFERENCE 4

Vector calculation for current (Amp) requirement for calculated thrust.

https://drive.google.com/drive/folders/1x4-jvrTwZFlh73j7YkdYLkvCjvKbguwV\

REFERENCE 5
Lithium Ion Battery: https://en.wikipedia.org/wiki/Lithium-ion_battery
Lithium Polymer Battery: https://en.wikipedia.org/wiki/Lithium_polymer_battery

Solid State Battery: https://en.wikipedia.org/wiki/Solid-state_battery

REFERENCE 6

Verification of propulsion & power system calculation by E-calc.

https://drive.google.com/file/d/1kxr12hKVcuxnv4N_B3W602hGN9sj6ERL/view?usp=sharing

REFERENCE 7

Various materials can be compared and selected using material selection charts, as shown in the Figure below. These charts provide a visual representation of different materials' properties, such as strength, density, corrosion resistance, and cost, enabling engineers and designers to make informed decisions when choosing materials for specific applications.

More such charts can be found from:

http://www-materials.eng.cam.ac.uk/mpsite/interactive_charts/
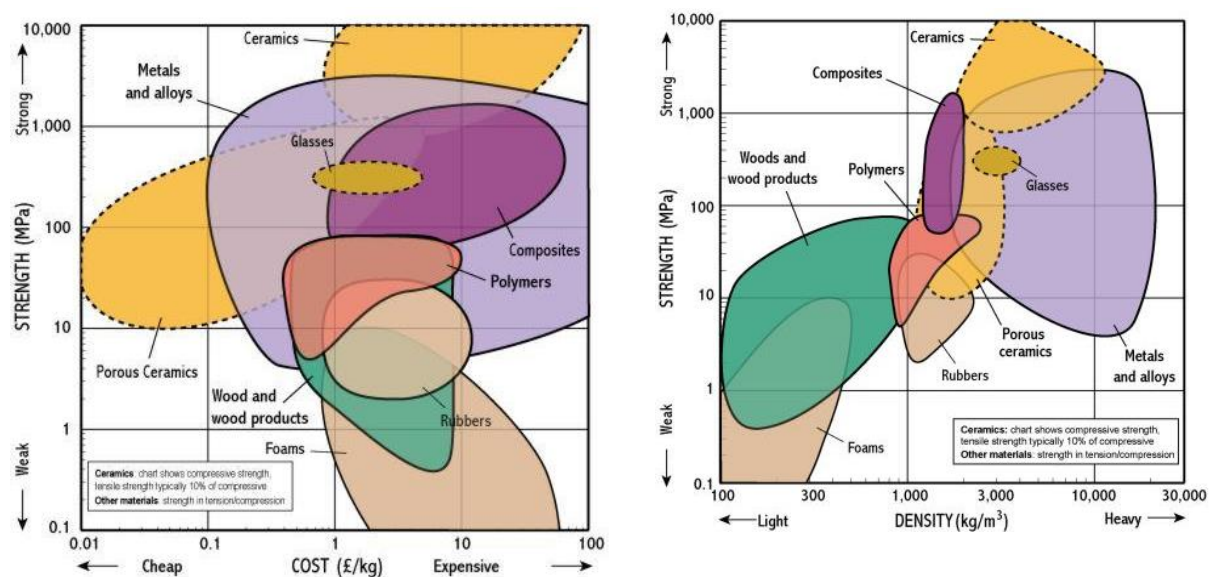
REFERENCE 8

Control System López, J. A., Dormido, R., Dormido, S., & Gómez, J. L. (2015). A Robust H Controller for an UAS Flight Control System. The Scientific World Journal, 2015, 1-11.

https://doi.org/10.1155/2015/403236

REFERENCE 9

Preliminary Moment Calculation

Sr. No.	Component	Weight (kg)	I(xx) (kg.mm^2)	I(yy) (kg.mm^2)	I(zz) (kg.mm^2)
1	Frame hub	0.1	0	16.0966875	0.3
2	Net Rotor Arm 1	0.04	21.33333333	5.219283	33.06056033
3	Net Rotor Arm 2	0.04	21.33333333	5.219283	33.06056033
4	Net Rotor Arm 3	0.04	21.33333333	5.219283	33.06056033
5	Net Rotor Arm 4	0.04	21.33333333	5.219283	33.06056033
6	GPS with stand	0.103	0	46.12988986	116.6351821

7	Pixhawk Cube Orange with damper	0.074	0	0.013875	85.86466667
8	Herelink	0.09	0	18.93796875	74.80512675
9	Herelink annetna	0.01	6.189160333	2.0172	10.53375408
10	Herelink annetna	0.01	6.189160333	2.0172	10.53375408
11	Motor number 1	0.06	107.809928	1.14005	143.752968
12	Motor number 2	0.06	107.809928	1.14005	143.752968
13	Motor number 3	0.06	107.809928	1.14005	143.752968
14	Motor number 4	0.06	107.809928	1.14005	143.752968
15	Camera	0.085	0	22.61977571	90.0313455
16	Safety Switch	0.007	0.00058333333	0.07714583333	3.733333333
17	Buzzer	0.007	0.5533733333	0.3645833333	2.640515733
18	ESC	0.0025	0	0.6188020833	0
19	Landin gear 1	0.014	0	8.796023717	3.637789867
20	Landing gear 2	0.014	0	8.796023717	3.637789867
21	Battery	0.55	0.103125	4.136458333	0.7333333333
22	Pixhawk Power Brick Mini	0.018	0	1.683375	13.5375
23	Wires	0.2	0	13.5375	0
24	Drop Mechanism	0.03	4.6225	5.36154025	0.015625
25	Payload	0.2	0	0	0
	Total	1.9145		534.2309477	176.6413811

Final UAS design moment calculation

Sr. No.	Component	Weight (kg)	I(xx) (kg.mm^2)	I(yy) (kg.mm^2)	I(zz) (kg.mm^2)
1	Frame hub	0.087	0	14.00411813	0.261
2	Net Rotor Arm 1	0.038	20.26666667	4.95831885	31.40753232
3	Net Rotor Arm 2	0.038	20.26666667	4.95831885	31.40753232
4	Net Rotor Arm 3	0.038	20.26666667	4.95831885	31.40753232
5	Net Rotor Arm 4	0.038	20.26666667	4.95831885	31.40753232
6	GPS with stand	0.1	0	44.78630083	54.45921333
7	Pixhawk Cube Orange with damper	0.074	0	0.013875	61.17432
8	Herelink	0.09	0	18.93796875	68.573883
9	Herelink annetna	0.01	8.333333333	2.0172	8.470560333
10	Herelink annetna	0.01	8.333333333	2.0172	8.470560333
11	Motor number 1	0.0613	100.5528931	1.164751083	115.3055942
12	Motor number 2	0.0613	100.5528931	1.164751083	115.3055942
13	Motor number 3	0.0613	100.5528931	1.164751083	115.3055942
14	Motor number 4	0.0613	100.5528931	1.164751083	115.3055942
15	Camera	0.085	0	22.61977571	67.54328438

No	Component				
16	SAFETY SWITCH	0.007	0.0005833333333	0.07714583333	3.733333333
17	Buzzer	0.007	0.5390933333	0.3645833333	2.640515733
18	ESC	0.0025	0	0.6188020833	0
19	Landin gear 1	0.014	0	8.796023717	3.637789867
20	Landing gear 2	0.014	0	8.796023717	3.637789867
21	Battery	0.45	0.15	3.384375	0.6081273375
22	Pixhawk Power Brick Mini	0.028	0	2.618583333	21.05833333
23	Wires	0.2	0	13.5375	0
24	Drop Mechanism	0.025	3.852083333	4.467950208	0.01302083333
25	Payload	0.2	0		0
Total		1.8007	504.4866657	171.5497054	891.1342379

REFERENCE 10

Cost Estimation

Sr. No.	Component	Cost
1	Top Plate	2,000
2	Bottom Plate	2,000
3	Arms	3,000
4	Bolts	1,500
5	Landing Gear	500
6	GPS Stand	1,900
7	Pixhawk Cube Orange	32,000
8	Herelink	91,000
9	Motors	12,800
10	Propeller	200
11	Camera	10,000
12	GPS	25,000
13	Buzzer & Safety Switch	700
14	ESC	6,000
15	Battery	5,219
16	UBEC	300
17	Wires	600
18	Drop Mechanism	5,000
Total		1,99,719

REFERENCE 11

Script reference

https://drive.google.com/drive/folders/1psYiOWkRADzFd-amXY106RvlN7i365mn?usp=sharing